Influence of Atmospheric Rivers on Alaskan River Ice

Russell Limber[1], Elias C. Massoud[2], Bin Guan[3], Forrest M Hoffman[4], and Jitendra Kumar[4]

[1]The University of Tennessee Knoxville
[2]Jet Propulsion Laboratory
[3]University of California Los Angeles
[4]Oak Ridge National Laboratory (DOE)

July 26, 2024

Abstract

Atmospheric rivers (ARs) transport vast amounts of moisture from low to high latitude regions. One region particularly impacted by ARs is Interior Alaska (AK). We analyze the impact of ARs on the annual river ice breakup date for 25 locations in AK. We
investigate the AR-driven rise in local air temperatures and explore the relationship between ARs and precipitation, including extremes and interannual variability. We found that AR events lead to an increase in local air temperatures for up to one week (by [?] 1°C). Interannually, ARs account for 36% of total precipitation, explain 48% of precipitation variability, and make up 57% of extreme precipitation events. By estimating the heat transfer between winter precipitation and the river ice surface, we conclude that increased precipitation during the coldest period of the year delays river ice breakup dates, while precipitation occurring close to the breakup date has little impact on breakup timing.

Influence of Atmospheric Rivers on Alaskan River Ice

Russ Limber[1,2], Elias C. Massoud[2], Bin Guan[3,4], Forrest M. Hoffman[2], Jitendra Kumar[2]

[1]The University of Tennessee, Knoxville, Knoxville, TN, USA
[2]Oak Ridge National Laboratory, Oak Ridge, TN, USA
[3]Joint Institute for Regional Earth System Science and Engineering, University of California, Los Angeles, CA, USA
[4]Jet Propulsion Laboratory, California Institute of Technology, Pasadena, CA, USA

Key Points:

- Interannually, atmospheric rivers (ARs) can lead to a week-long persistent increase in daily air temperatures over Interior Alaska (AK)
- In AK, ARs account for 36% of annual precipitation, 57% of extreme precipitation and explain 48% of interannual variability of precipitation
- AR events during the coldest months delay the annual breakup date of river ice, while ARs closer to the breakup date have less impact

Corresponding author: Russ Limber, r62@ornl.gov

Abstract

Atmospheric rivers (ARs) transport vast amounts of moisture from low to high latitude regions. One region particularly impacted by ARs is Interior Alaska (AK). We analyze the impact of ARs on the annual river ice breakup date for 25 locations in AK. We investigate the AR-driven rise in local air temperatures and explore the relationship between ARs and precipitation, including extremes and interannual variability. We found that AR events lead to an increase in local air temperatures for up to one week (by ≈ 1 °C). Interannually, ARs account for 36% of total precipitation, explain 48% of precipitation variability, and make up 57% of extreme precipitation events. By estimating the heat transfer between winter precipitation and the river ice surface, we conclude that increased precipitation during the coldest period of the year delays river ice breakup dates, while precipitation occurring close to the breakup date has little impact on breakup timing.

Plain language summary

Atmospheric rivers (ARs) are large storm systems originating in tropical regions capable of depositing large amounts of precipitation in high latitude regions. Using river ice breakup data recorded throughout Interior Alaska (AK) we set out to explore the relationship between ARs and annual river ice breakup timing from 1980 to 2023. We found that daily air temperature increases can last up to one week after an AR event. Interannually, ARs account for 36% of total precipitation, explain 48% of the variability of precipitation, and make up 57% of extreme precipitation events. We then approximated the total heat transfer between precipitation and the river ice surface. We used the mass and temperature of precipitation accumulated on the river ice surface to approximate thermal energy exchange. The magnitude of energy exchange was then correlated to river ice breakup timing. We found that greater amounts of precipitation from both AR and non-AR induced precipitation, occuring relatively close to river ice breakup dates, have little correlation to the breakup date. However, increased precipitation during the coldest period of the year (typically late December to early February) is strongly inversely correlated with river ice breakup timing and seems to delay the breakup date.

1 Introduction

Atmospheric rivers (ARs) are narrow corridors of intense water vapor that significantly influence hydrologic events, transporting most of the water vapor outside of the Tropics (American Meteorological Society, 2024). It is estimated that ARs are responsible for as much as 90% of poleward water vapor transport at midlatitudes (Zhu & Newell, 1998). ARs contribute to extreme precipitation events across various regions worldwide (Espinoza et al., 2018; Massoud et al., 2019), including Western North America (Dettinger et al., 2004; Neiman et al., 2008; Guan et al., 2010; Paul J. et al., 2011; Ralph et al., 2006; F. Martin et al., 2019; Dettinger et al., 2011) Europe (Lavers et al., 2013; Harald & Andreas, 2013), the Middle East (Massoud et al., 2020; Lashkari & Esfandiari, 2020; Esfandiari & Shakiba, 2024), and Western South America (Viale et al., 2018). In recent years, the impacts of ARs on the cryosphere such as Greenland (Mattingly et al., 2018) and Antarctica (Gorodetskaya et al., 2014; Wille et al., 2021; Maclennan et al., 2022a), have been more extensively analyzed. In addition, a growing number of works investigating the relationship between ARs and high latitude regions have been undertaken (Hegyi & Taylor, 2018; Wang et al., 2024). Evidence shows that between 1981 and 2020, higher atmospheric moisture content was significantly correlated with lower sea ice coverage over almost the entire Arctic Ocean (Li et al., 2022). For those same years, another analysis found that 100% of extreme temperature events in the Arctic (above 0 °C) coincide with the presence of ARs (Ma et al., 2023). Analyses have noted a relationship between frequent AR activity and sea ice loss, caused by increased rainfall from moisture originating in lower latitudes (Zhang et al., 2023; Maclennan et al., 2022b). However, Arctic systems are complicated, as the intense moisture transport within ARs can also result in heavy snowfall events, thus contributing to the accumulation of snowpack, especially in mountainous regions (Saavedra et al., 2020; Guan et al., 2010). Under the right conditions, this relationship has been found to actually increase the mass balance of glaciers. Little et al. (2019) found ARs to be the primary drivers of both highest ablation and snowfall events, substantially impacting glacier mass balance at Brewster Glacier in New Zealand. Understanding the role of ARs in the cryosphere is essential for assessing their broader impact on regional water resources and glacier dynamics in a changing climate.

While a number of works have explored the relationship between ARs and sea ice, glaciers, and ice sheets, to our knowledge there has been no study that investigates the relationship between ARs and Arctic river ice. Past studies have used physics based processes to model the annual breakup timing and conditions of Arctic river ice (Paily et al., 1974; G. Ashton, 1986; T. Prowse et al., 2007; Jasek, 1998; Shen, 2010). Through such studies, it is recognized that an increase in precipitation leads to an increase in streamflow, altering the hydraulics associated with river ice breakup, and potentially accelerating mechanical breakup events (G. Ashton, 1986). It has also been proposed that increased snow pack as a result of increased precipitation contributes to breakup severity (T. D. Prowse & Beltaos, 2002). Using breakup records throughout Interior Alaska (AK) from the Alaska-Pacific River Forecast Center Database (the same breakup records used in this analysis) Bieniek et al. (2011) determined that winter precipitation plays a relatively minor role in impacting the breakup timing of river ice and if anything accelerates the breakup timing as a result of increased streamflow. They also report that increased storm activity in the spring leads to increased surface air temperature, leading to earlier breakup dates (Bieniek et al., 2011). However, their analysis used only 4 sites (as opposed to the 25 used in this analysis) and aggregated precipitation seasonally, without accounting for the interaction between winter precipitation and temperature that occurs at a finer temporal resolution.

Our analysis aims to answer the following questions: 1.) Since ARs have been known to impact Arctic systems by increasing temperatures, is there a change in air temperature in different regions of AK corresponding to the presence of ARs? 2.) How do ARs contribute to precipitation throughout AK, considering how ARs impact total annual precipitation, interannual variability, and extreme events? 3.) How do ARs impact the timing of river ice breakup, does the presence of ARs accelerate or delay the timing of river ice breakup?

2 Data

2.1 Atmospheric Rivers Catalog

Similar to previous studies, we define ARs using integrated vapor transport (IVT) constructed from 6-hourly values of 3-D wind and water vapor at eight pressure levels between 300 and 1,000 mb from the National Center for Environmental Protection (NCEP) reanalysis data product (Kalnay et al., 1996). AR detection is based on version 3 of the tARget algorithm (Guan & Waliser, 2019; Guan, 2022). The IVT values are calculated at the original resolution from the NCEP meteorological inputs (Saha et al., 2010). Guan and Waliser (2015) developed a global AR detection algorithm, which was updated and validated later with dropsonde data (Bin et al., 2018). This algorithm is employed in our study, which is based on a combination of IVT magnitude, direction, and geometry characteristics, to objectively identify ARs. Contiguous regions of enhanced IVT transport are first identified from magnitude thresholding (i.e. grid cells above the seasonally and locally dependent 85^{th} percentile, or $100\frac{\text{kg}}{\text{m}*\text{s}}$, whichever is greater) and further filtered using directional and geometry criteria requirements. Although the $100\frac{\text{kg}}{\text{m}*\text{s}}$ threshold is applied globally, it is intended for dry (including polar) regions since in other regions the 85^{th} percentile is already larger than $100\frac{\text{kg}}{\text{m}*\text{s}}$. The detection algorithm was applied to

NCEP reanalysis data at its native resolution of 2.5°. This detection algorithm had over 90% agreement in detecting AR landfall dates when compared with other AR detection methods for Western North America (Neiman et al., 2008), the United Kingdom (Lavers et al., 2011), and East Antarctica (Gorodetskaya et al., 2014).

2.2 Daymet Daily Surface Weather and Climatological Summaries

Daily minimum ($T_{\min}$) and maximum ($T_{\max}$) temperatures and precipitation data were obtained from Daymet (M. Thornton et al., 2022). Daymet provides continuous and gridded estimates of daily weather at 1km × 1km resolution. Daymet precipitation, $T_{\min}$ and $T_{\max}$, were selected in this analysis due to their strong agreement with NCEP temperature time series for our region of interest (Figure 1C). Daymet is derived by interpolating and extrapolating from in situ instruments and meteorological stations, and represents a robust dataset for precipitation and temperature predictions across North America (P. E. Thornton et al., 2021). This dataset has been a standard for validation among several analyses related to arctic regions (Diro & Sushama, 2019; Akinsanola et al., 2024). Figure 1 (A, B) show the annual mean precipitation and temperature for the year 2021 across Alaska. For one of the study locations, Crooked Creek at the Kuskokwim River, Figure 1 (C) shows the time series of precipitation, temperature and AR events for the year 2021.

2.3 River ice breakup observations

Observations for river ice breakup dates were obtained from the Alaska-Pacific River Forecast Center database. While exact coordinates were unavailable, location coordinates were estimated based on proximity to weather stations and airports, to maintain spatial consistency with inputs used in Daymet's meteorological models. We identified 25 locations (shown in Figure 1 (A, B)) in the database that had at least 35 breakup records between 1980 and 2023 (the current temporal availability of Daymet), although breakup records go as far back as 1896 for some locations. The 35 breakup records threshold was used because it allowed for the greatest number of locations with the most complete time series necessary for statistical analysis. There is always one breakup date per year, but not every year had a recorded date, so some years are represented as empty values in the dataset. On average, recorded breakup dates range from mid-March to late-June This dataset has been used in several other studies such as (Murphy et al., 2022; Brown et al., 2018; Bieniek et al., 2011). As an example, the breakup date for Crooked Creek at the Kuskokwim River in 2021 occurred in early-May and is depicted in Figure 1 (C) with a vertical purple dashed line.

3 Methods

To assess the influence of ARs on local temperature, we analyze the relationship between the presence of an AR and the temperature change at a specific location. The presence of an AR is represented numerically as a binary value indicating whether or not an AR is active on a particular date. We then estimate how many days this change in temperature persists. To do this, we conducted a pairwise t-test using a varying temporal window. In other words, for each AR occurrence in the dataset, a pre–AR time window and post–AR time window each equal to n days in length was created before and after the AR event date, respectively, whereby: $n \in \{1, 2, 3, \ldots, 14\}$. For values of n greater than one day the mean was calculated within each time window for $T_{\min}$ and $T_{\max}$. These averaged temperatures were then calculated over all locations. Mean temperature pairs were assessed using a one tailed pairwise t-test to check whether ARs increased the local temperature over period of time n ($\alpha = 0.05$). For example, if $n = 3$ assessing $T_{\min}$, then the mean of $T_{\min}$ three days prior to each AR event will be compared to the mean of $T_{\min}$ for the three days post each AR event.

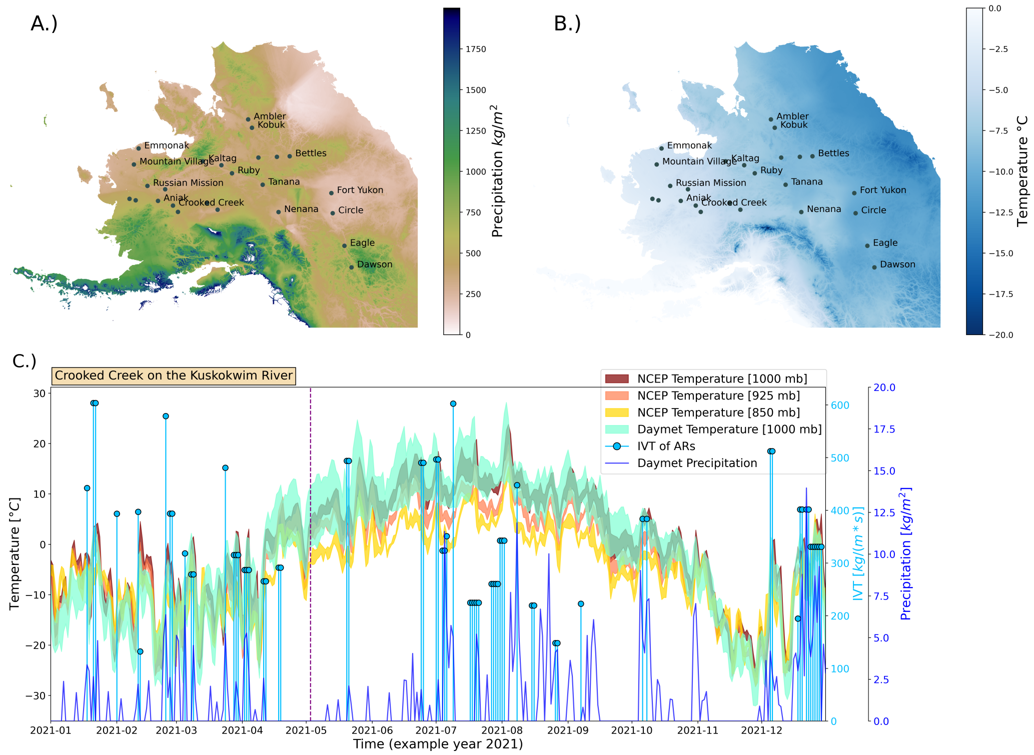

Figure 1. (A): map shows annual total precipitation for the year 2021. (B): map of average daily temperature for 2021. (C): One of the 25 locations (Crooked Creek on the Kuskokwim River) for the year 2021. Yellow, orange, red represent the temperature profiles (fill plot of T_{min} - T_{max}) from NCEP temperature data at 850, 925 and 1000mb respectively. Light green represents the Daymet temperature profile. Dark blue line shows precipitation from Daymet ($\frac{\text{kg}}{\text{m}^2}$) relative to the secondary y-axis in dark blue on the right. The light blue stem plots depict the IVT of AR events ($\frac{\text{kg}}{\text{m}*\text{s}}$) relative to the secondary y-axis in light blue on the right. The vertical purple dashed line shows the breakup date for the Kuskokwim River in 2021 for Crooked Creek.

We explored AR contribution to precipitation by seperating precipitation events occuring on days with an active AR. We then used the Wilcoxon rank-sum test (Rey & Neuhauser, 2011) to test the hypothesis that AR events tend to produce more precipitation than other precipitation events. We opted to use a non-parametric test (Wilcoxon rank-sum test) because the distributions of precipitation were shown to not be normal after log transformation using the Shapiro-Wilks test (Shapiro & Wilk, 1965). We also estimated the interannual variability of precipitation associated with ARs by conducting a univariate ordinary least squares regression (OLS). For extremes, we extracted the top 5% of precipitation events and determined what fraction of those events occured on days with an active AR event.

To determine the impact that ARs have on river ice breakup timing, we estimate the heat transfer between the river ice and the precipitation accumulating on the surface. Assuming presence of a frozen layer of ice on the river surface, we estimate the sensible heat transfer between the river surface and incoming precipitation using Equation 1. Latent heat transfer fluxes were assumed to be relatively small and thus ignored in our simplified heat transfer calculations. The specific heat of precipitation in Equation 1 is represented as either water or liquid as determined by air temperature. Given that Alaska is at a high latitude with heat transfer calculated during the coldest period of the year, it can be assumed that in most cases the precipitation is in the form of snow.

$$q_t = \rho \cdot m \cdot \Delta T \tag{1}$$

where q_t is heat flux ($\frac{\text{J}}{\text{m}^2}$) at a given day t; ρ the specific heat of the precipitation (assumed to be either water or snow depending on the temperature) ($\frac{\text{J}}{\text{kg°C}}$); ΔT is the difference between the temperature of the precipitation which is approximated using T_{min} as a proxy, and the river ice surface which is assumed to be at 0 °C; m the mass of the precipitation per unit area ($\frac{\text{kg}}{\text{m}^2}$).

Heat transfer fluxes were calculated as a daily series for a period of six months prior to the breakup date. Time of occurrence and thermal conditions associated with precipitation events during winter and spring have differential impacts to reinforce versus weaken the river ice layer and thus the date of the breakup. We fit a temporal bias function (Equation 2), a double exponential function, applied to the heat transfer equation to assess the days of the year when precipitation events were more impactful on breakup timing. The bias function is a symmetric unimodal exponential function to help identify the most influencial precipitation time period determining the annual time of river ice breakup. This bias function was fit individually for each of the study locations.

$$f(t; \gamma, \kappa, DOY, c) = \begin{cases} \frac{e^{-\gamma\cdot(-t-DOY)}-1}{\kappa} & \text{if } t < c \\ \frac{e^{-\gamma\cdot(t-DOY)}-1}{\kappa} & \text{if } t \geq c \end{cases} \tag{2}$$

where γ is a scale parameter impacting the width of the exponential function; t is time in days; DOY is the Gregorian day of year that the breakup date occurred; c is a location parameter dictating the center placement of the function; κ is a normalizing constant. Finally, Equation 3 solves for $Q_{\text{year, location}}$, the total thermal energy exchange for a given location, for a given breakup year. Equation 3 is tuned over the entire hyperparameter search space for each location and each breakup year, optimized by selecting the parameter values that produce the Pearson correlation coefficient with the greatest absolute value. Here i is the starting day of the time series approximately six months prior to the breakup date.

$$Q_{\text{year, location}} = \sum_{t=i}^{t=DOY} f(t; \gamma, \kappa, DOY, c) \cdot q_t \tag{3}$$

4 Results

4.1 Atmospheric rivers impact on temperature

We applied the pairwise t-test comparing pre–AR and post–AR time windows of length n at all locations. Figures 2A and 2B show the change in p-values for each value of n where the dashed lines represent the mean p-value across the study locations and the filled color curved signifies the interquartile range (IQR). Figure 2C and 2D shows the mean increase in temperature from the pre–AR time window to the post–AR time window for varying time window sizes n. Analysis shows an increase in air temperature during the period following an AR event, with mean temperature increases higher for $T_{\min}$ compared to $T_{\max}$, with the difference receding over longer time windows. On average, the temperature differences were statistically significant for $T_{\min}$ (based on an $\alpha = 0.05$) for temporal windows up to 10 days after an AR event. For temporal windows up to 7 days, statistical significance was true for all locations within the study as represented by the Figure 2A fill plot. The increase in daily minimum temperature can be as high as 1.5 °C ($n = 2$) (Figure 2C). For $T_{\max}$, the differences were statistically significant for up to 6 days after an AR event on average (Figure 2B) with an increase as high as 0.75 °C ($n = 3, 4$) (Figure 2D). These statistically significant temperature increases following AR events were true at all locations in our study for $n = 2, 3, 4$ as shown in Figure 2B fill plot.

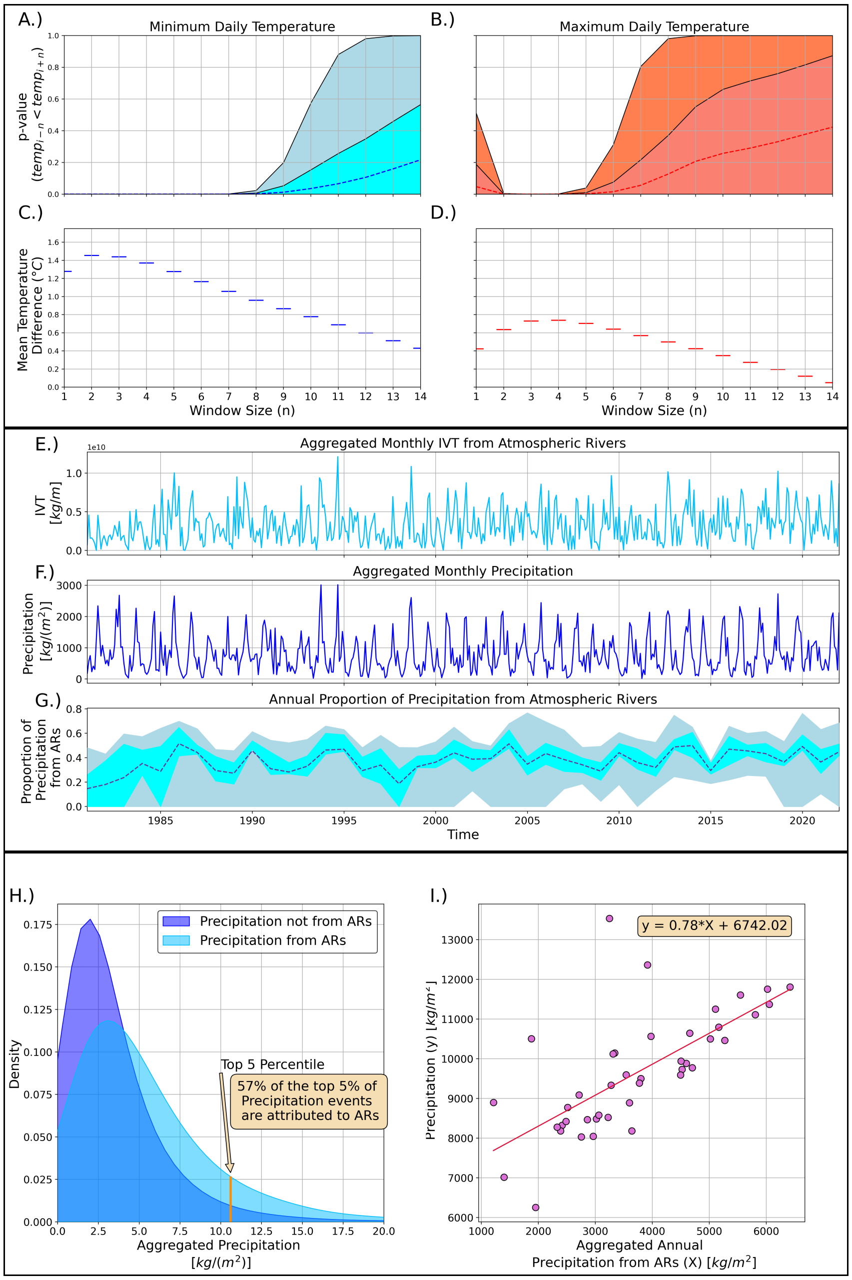

Figure 2. (A and B): p-values from the paired t-test given time window size (n) surrounding the AR event date (A: $T_{\min}$; B: $T_{\max}$). Dashed lines represent the mean, while the filled color curves show interquartile range (25th and 75th percentile); (C and D): mean increase in temperature (°C) accompanying each AR, calculated between the pre–AR time window and the post–AR time window (C: $T_{\min}$; D: $T_{\max}$). (E): time series of IVT $\frac{\text{kg}}{\text{m}}$ aggregated monthly over all locations. (F): time series of total precipitation $\frac{\text{kg}}{\text{m}^2}$ aggregated monthly over all study locations. (G): proportion of precipitation accounted for by ARs on an annual basis. (H): kernel density plots showing the distribution of local precipitation (dark blue) and precipitation from ARs (light blue). (I): ordinary least squares regression plot using total annual precipitation from ARs, to predict total annual precipitation.

4.2 Atmospheric rivers impact on precipitation

Figures 2E and 2F show the monthly IVT from AR events and monthly total precipitation through the span of the data record, aggregated over all locations, respectively. Figure 2G shows the proportion of total annual precipitation occuring on days with active ARs over time, where light blue depicts the IQR of proportions and blue-grey represents proportions outside of the IQR, across all 25 locations. The dashed line represents the mean proportion. ARs tend to account for 36% of precipitation on average (Figure 2G), with a high degree of variability across years and locations. In 2005 and 2020 for example, nearly 80% of the total precipitation at some locations occured on days with active AR events. The results from the Wilcoxon rank-sum test show that precipitation during active ARs tends to be greater in magnitude than non-AR precipitation (test statistic = -83.85; p-value ≈ 0.0). In addition, we found that of the top 5% of precipitation events by total rainfall, 57% occured during active ARs (Figure 2H). Correlating total precipitation from AR days, to total annual precipitation using a univariate OLS, we find that the coefficient of determination (R^2) is equal to 0.48 (Figure 2I). This indicates that ARs explain about 48% of interannual variability in precipitation, across all 25 locations.

4.3 Transfer of energy based on Precipitation

To estimate the impact of precipitation on river ice breakup dates, we use Equation 3 to approximate the heat transfer between precipitation and the river ice surface. Equation 3 was solved using a double exponential bias function to temporally-weigh events of higher influence (Figures 3A, 3B, 3C), and using uniform weights as baseline for comparison (Figures 3D, 3E, 3F). When using a temporal bias function, the relationship between summated heat transfer due to precipitation and time of river ice breakup were identified with strong correlation (Pearson correlation coefficient (r_p) = -0.84 and a Spearman correlation coefficient (r_s) = -0.80 at Crooked Creek on the Kuskokwim river (Figure 3A)). In contrast, very weak correlations were identified when fitting the relationship using temporally uniform weights (Figure 3B), thus highlighting the need for a temporal bias function. We tuned three different cases for Equation 1 whereby the mass of precipitation could be provided by: total precipitation, precipitation from ARs or precipitation not from ARs. This exercise allows us to determine whether or not that aggregated energy accelerates or decelerates the breakup of river ice. We find that there is a strong negative correlation between the heat transfer and the DOY on which the river ice breakup occurs (Figure 3A). In this context, negative values along the y-axis of Figures 3A and 3D are interpreted as a negative heat exchange, suggesting a net cooling effect on the river ice surface as the precipitation below freezing are accumulated on the river ice surface. The peak of the temporally-weighted bias curve is typically located during the coldest period of the year, typically betweeen late November and early February (Figure 3C). In other words, the presence of high magnitude precipitation events, occuring on colder days of the year, show a strong inverse correlation to the time of breakup. For example, referring to Figure 3A, Crooked Creek on the Kuskokwim River has a clear negative trend, whereby the cooling effect of precipitation on the river ice surface delays the DOY of the breakup. The frequency of AR events that occurred six months prior to the breakup date alone is an insufficient predictor (Figures 3B, 3E) of the breakup date.

While Figure 3 focuses on a single selected site, Table 1 shows the Pearson correlation after tuning parameters c and γ are optimized and applied to Equation 3 individually at each location. Table 1 also shows the center of the bias curve c (month-day) that was selected for, at each location, given the summand for precipitation used in Equation 3 (ie. Total Precipitation, Precipitation from ARs, Precipitation not from ARs; mulitplied to the temporal bias).

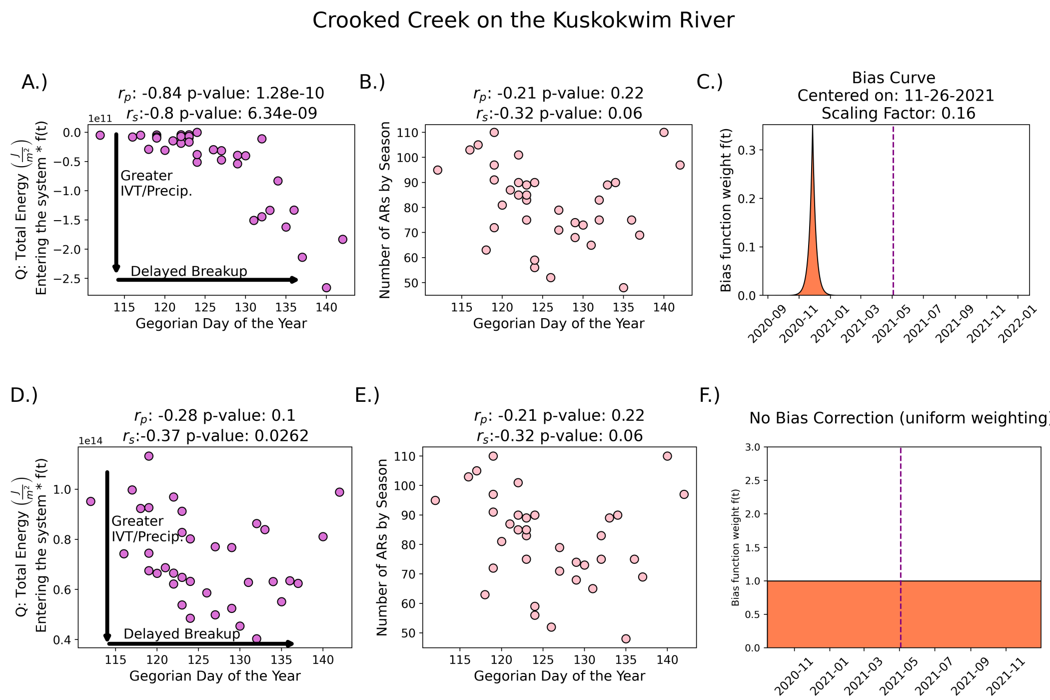

Figure 3. top row: (A): scatter plot between thermal energy transfer for all precipitation events and DOY (the Gregorian day of year that the breakup date occurred); (B): scatter plot of the number of ARs that occured in the six months prior to the breakup date and DOY; (C): temporal bias curve for the year 2021 with the breakup date represented by the vertical dashed line. bottom row: same as the top row except depicting the results when a temporal bias is not utilized.

5 Conclusion and Discussion

This study investigated the impact atmospheric rivers (ARs) and non-AR related precipitation events have on the timing of river ice breakup across 25 sites in Alaska. We explored the impact of ARs on local temperature increases throughout the study domain; the contribution of ARs to precipitation events, including variability and extremes; and determined the impact of ARs and non-AR precipitation events on the DOY on which the ice on the surface of Alaskan rivers eventually breaks.

We found that ARs generally lead to up to a week-long persistent increase in daily temperature (minimum and maximum) across Alaska, with temperatures rising by as much as 1.5 °C for $T_{\min}$ and 0.75 °C for $T_{\max}$. These findings are consistent with many past studies that have shown that warm moisture and an increase in heat flux brought on by ARs can warm the cryosphere (Wille et al., 2021; Ma et al., 2023; Li et al., 2022; Zhang et al., 2023). Our analysis also shows that ARs account for a significant portion of total annual precipitation in Alaska, contributing to 36% of total precipitation by volume on average. ARs also explain 48% of interannual variability and lead to 57% of extreme precipitation events (precipitation events within the top 5% of deposition). These results are consistent with past works, such as Nash et al. (2024) which showed that throughout Southeast Alaska, as few as six annual AR events can account for 68% - 91% of precipitation days. Our analysis shows evidence that intense ARs occurring during the coldest period of the year appear to delay the annual breakup date of river ice. Our results do not show that ARs are unique relative to non-AR forms of precipitation in this regard (Table 1), with no evidence that increased precipitation events of any kind closer to the breakup date accelerates the breakup date. This is likely attributed to a combination of heat transfer from precipitation, increased ice accumulation on the river ice surface and structural changes in the river ice as a result of snowfall. Increased snow accumulation increases the albedo of the river surface, as well as provides thermal insulation, mitigating the effects of temperature fluctuations during the coldest period of the year. This is consistent with the extensive analysis conducted by G. D. Ashton (2011), showing that an increase in snow accumulation on the river ice surface for locations across Alaska (many of the same locations used in this analysis) can lead to an increase in river ice thickness, thus reinforcing the river ice structurally. This phenomenon is apparent to a point at which the efficacy begins to diminish. It should be noted that a limitation of our analysis is the assumption that the river ice surface temperature is held constant at 0 °C and that air temperature is a reasonable proxy for incoming precipitation. We were unable to find a complete dataset on river ice surface temperatures for the locations and time period of our study. Thus, we assume that the mass of liquid, snow or ice deposited on the river surface, times its temperature and specific heat, will be sufficient to approximate the heat exchanged in the system.

Understanding the influence of ARs and other high precipitation events on the timing of river ice breakup in Alaska is crucial for predicting and managing the impacts of climate change in the region, especially since studies have shown that AR frequency and intensity in this region are expected to increase in a warmer world (Espinoza et al., 2018; Massoud et al., 2019). The findings of our analysis suggests that ARs have significant influence on the climate and terrestrial hydrology across Alaska, affecting temperature, precipitation, and river ice dynamics. Further research in this area could help improve our understanding of ARs and their role in shaping the climate of high-latitude regions.

Data Availability Statement

Daily Daymet precipitation and temperature data is available through the Oak Ridge National Laboratory Distributed Active Archive at `https://daymet.ornl.gov/single-pixel/`. River ice breakup records are maintained by the Alaska-Pacific River Forecast Center at `https://www.weather.gov/aprfc/breakupMap`. The AR database (`https://doi.org/10.25346/S6/YO15ON`) is available via the Global Atmospheric Rivers Dataverse at `https://dataverse.ucla.edu/dataverse/ar`. NCEP-NCAR Reanalysis 1 data was obtained from the NOAA Physical Sciences Laboratory, Boulder, Colorado, USA, `https://psl.noaa.gov/data/index.html`. All of the codes needed to run the analysis and everything required to reproduce this work are available on GitHub: `https://github.com/Russtyhub/River_Ice_AR_Analysis.git`.

Acknowledgments
This work was supported by the U.S. Department of Energy, Office of Science, Biological and Environmental Research (BER) Regional and Global Model Analysis (RGMA) program, as part of The Interdisciplinary Research for Arctic Coastal Environments (InteRFACE) project. Development of the AR database was supported by NASA and the California Department of Water Resources. This manuscript has been authored in part by UT-Battelle, LLC, under contract DE-AC05-00OR22725 with the US Department of Energy (DOE). The publisher acknowledges the US government license to provide public access under the DOE Public Access Plan (http://energy.gov/ downloads/doe-public-access-plan).

References

Akinsanola, A. A., Jung, C., Wang, J., & Kotamarthi, V. R. (2024). Evaluation of precipitation across the contiguous united states, alaska, and puerto rico in multi-decadal convection-permitting simulations. *Scientific Reports*, *14*(1), 1238. Retrieved from https://doi.org/10.1038/s41598-024-51714-3 doi: 10.1038/s41598-024-51714-3

American Meteorological Society. (2024). *Glossary of meteorology: Atmospheric river.* Retrieved from https://glossary.ametsoc.org/wiki/Atmospheric_river?__cf_chl_tk=LTK3vMNlWxxKfhHCGpS05IMiQaNMnEAledLyvfTD7T0-1717350416-0.0.1.1-4330 (Accessed: 2024-06-03)

Ashton, G. (1986). *River and lake ice engineering*. Water Resources Publications. Retrieved from https://books.google.com/books?id=xglYVjAsnt8C

Ashton, G. D. (2011). River and lake ice thickening, thinning, and snow ice formation. *Cold Regions Science and Technology*, *68*(1), 3-19. Retrieved from https://www.sciencedirect.com/science/article/pii/S0165232X11000875 doi: https://doi.org/10.1016/j.coldregions.2011.05.004

Bieniek, P. A., Bhatt, U. S., Rundquist, L. A., Lindsey, S. D., Zhang, X., & Thoman, R. L. (2011). Large-scale climate controls of interior alaska river ice breakup. *Journal of Climate*, *24*(1), 286 - 297. Retrieved from https://journals.ametsoc.org/view/journals/clim/24/1/2010jcli3809.1.xml doi: 10.1175/2010JCLI3809.1

Bin, G., Duane E., W., & F. Martin, R. (2018). An intercomparison between reanalysis and dropsonde observations of the total water vapor transport in individual atmospheric rivers. *Journal of Hydrometeorology*, *19*(2), 321 - 337. Retrieved from https://journals.ametsoc.org/view/journals/hydr/19/2/jhm-d-17-0114_1.xml doi: 10.1175/JHM-D-17-0114.1

Brown, D. R. N., Brinkman, T. J., Verbyla, D. L., Brown, C. L., Cold, H. S., & Hollingsworth, T. N. (2018). Changing river ice seasonality and impacts on interior alaskan communities. *Weather, Climate, and Society*, *10*(4), 625 - 640. Retrieved from https://journals.ametsoc.org/view/journals/wcas/10/4/wcas-d-17-0101_1.xml doi: 10.1175/WCAS-D-17-0101.1

Dettinger, M. D., Cayan, D. R., Meyer, M. K., & Jeton, A. E. (2004). Simulated hydrologic responses to climate variations and change in the merced, carson, and american river basins, sierra nevada, california, 1900–2099. *Climatic Change*, *62*(1), 283–317. Retrieved from https://doi.org/10.1023/B:CLIM.0000013683.13346.4f doi: 10.1023/B:CLIM.0000013683.13346.4f

Dettinger, M. D., Ralph, F. M., Das, T., Neiman, P. J., & Cayan, D. R. (2011). Atmospheric rivers, floods and the water resources of california. *Water*, *3*(2), 445–478. Retrieved from https://www.mdpi.com/2073-4441/3/2/445 doi: 10.3390/w3020445

Diro, G. T., & Sushama, L. (2019). Simulating canadian arctic climate at convection-permitting resolution. *Atmosphere*, *10*(8). Retrieved from https://www.mdpi.com/2073-4433/10/8/430 doi: 10.3390/atmos10080430

Esfandiari, N., & Shakiba, A. (2024). The extraordinary atmospheric rivers analysis over the middle east: Large-scale drivers, structure, effective sources, and precipitation characterization. *Dynamics of Atmospheres and Oceans*, *105*, 101430. Retrieved from https://www.sciencedirect.com/science/article/pii/S0377026523000817 doi: https://doi.org/10.1016/j.dynatmoce.2023.101430

Espinoza, V., Waliser, D. E., Guan, B., Lavers, D. A., & Ralph, F. M. (2018). Global analysis of climate change projection effects on atmospheric rivers. *Geophysical Research Letters*, *45*(9), 4299-4308. Retrieved from https://agupubs.onlinelibrary.wiley.com/doi/abs/10.1029/2017GL076968 doi: https://doi.org/10.1029/2017GL076968

F. Martin, R., Jonathan J., R., Jason M., C., Michael, D., Michael, A., David, R., . . . Chris, S. (2019). A scale to characterize the strength and impacts of atmospheric rivers. *Bulletin of the American Meteorological Society*, *100*(2), 269 -

289. Retrieved from `https://journals.ametsoc.org/view/journals/bams/100/2/bams-d-18-0023.1.xml` doi: 10.1175/BAMS-D-18-0023.1

Gorodetskaya, I. V., Tsukernik, M., Claes, K., Ralph, M. F., Neff, W. D., & Van Lipzig, N. P. M. (2014). The role of atmospheric rivers in anomalous snow accumulation in east antarctica. *Geophysical Research Letters*, *41*(17), 6199-6206. Retrieved from `https://agupubs.onlinelibrary.wiley.com/doi/abs/10.1002/2014GL060881` doi: https://doi.org/10.1002/2014GL060881

Guan, B. (2022). *[Data] Global Atmospheric Rivers Database, Version 3.* UCLA Dataverse. Retrieved from `https://doi.org/10.25346/S6/YO15ON` doi: 10.25346/S6/YO15ON

Guan, B., Molotch, N. P., Waliser, D. E., Fetzer, E. J., & Neiman, P. J. (2010). Extreme snowfall events linked to atmospheric rivers and surface air temperature via satellite measurements. *Geophysical Research Letters*, *37*(20). Retrieved from `https://agupubs.onlinelibrary.wiley.com/doi/abs/10.1029/2010GL044696` doi: https://doi.org/10.1029/2010GL044696

Guan, B., & Waliser, D. (2019, 12). Tracking atmospheric rivers globally: Spatial distributions and temporal evolution of life cycle characteristics. *Journal of Geophysical Research: Atmospheres*, *124*. doi: 10.1029/2019JD031205

Guan, B., & Waliser, D. E. (2015). Detection of atmospheric rivers: Evaluation and application of an algorithm for global studies. *Journal of Geophysical Research: Atmospheres*, *120*(24), 12514-12535. Retrieved from `https://agupubs.onlinelibrary.wiley.com/doi/abs/10.1002/2015JD024257` doi: https://doi.org/10.1002/2015JD024257

Harald, S., & Andreas, S. (2013). Moisture origin and meridional transport in atmospheric rivers and their association with multiple cyclones. *Monthly Weather Review*, *141*(8), 2850 - 2868. Retrieved from `https://journals.ametsoc.org/view/journals/mwre/141/8/mwr-d-12-00256.1.xml` doi: 10.1175/MWR-D-12-00256.1

Hegyi, B. M., & Taylor, P. C. (2018). The unprecedented 2016–2017 arctic sea ice growth season: The crucial role of atmospheric rivers and longwave fluxes. *Geophysical Research Letters*, *45*(10), 5204-5212. Retrieved from `https://agupubs.onlinelibrary.wiley.com/doi/abs/10.1029/2017GL076717` doi: https://doi.org/10.1029/2017GL076717

Jasek, M. (1998, July 27–31). 1998 break-up and flood on the yukon river at dawson – did el niño and climate change play a role? In H. Shen (Ed.), *Ice in surface waters: Proceedings of the 14th international symposium on ice* (pp. 761–768). Rotterdam: A.A. Balkema.

Kalnay, E., Kanamitsu, M., Kistler, R., Collins, W., Deaven, D., Gandin, L., ... Joseph, D. (1996). The ncep/ncar 40-year reanalysis project. *Bulletin of the American Meteorological Society*, *77*(3), 437 - 472. Retrieved from `https://journals.ametsoc.org/view/journals/bams/77/3/1520-0477_1996_077_0437_tnyrp_2_0_co_2.xml` doi: 10.1175/1520-0477(1996)077⟨0437:TNYRP⟩2.0.CO;2

Lashkari, H., & Esfandiari, N. (2020, 05). Identifying atmospheric river events and their paths into iran. *Theoretical and Applied Climatology*, *140*. doi: 10.1007/s00704-020-03148-w

Lavers, D. A., Allan, R. P., Villarini, G., Lloyd-Hughes, B., Brayshaw, D. J., & Wade, A. J. (2013). Future changes in atmospheric rivers and their implications for winter flooding in britain. *Environmental Research Letters*, *8*(3). Retrieved from `https://doi.org/10.1088/1748-9326/8/3/034010` doi: 10.1088/1748-9326/8/3/034010

Lavers, D. A., Allan, R. P., Wood, E. F., Villarini, G., Brayshaw, D. J., & Wade, A. J. (2011). Winter floods in britain are connected to atmospheric rivers. *Geophysical Research Letters*, *38*(23). Retrieved from `https://agupubs.onlinelibrary.wiley.com/doi/abs/10.1029/2011GL049783` doi:

https://doi.org/10.1029/2011GL049783

Li, L., Cannon, F., Mazloff, M. R., Subramanian, A. C., Wilson, A. M., & Ralph, F. M. (2022). Impact of atmospheric rivers on arctic sea ice variations. *EGUsphere*, *2022*, 1–21. Retrieved from https://egusphere.copernicus.org/preprints/2022/egusphere-2022-36/ doi: 10.5194/egusphere-2022-36

Little, K., Kingston, D. G., Cullen, N. J., & Gibson, P. B. (2019). The role of atmospheric rivers for extreme ablation and snowfall events in the southern alps of new zealand. *Geophysical Research Letters*, *46*(5), 2761-2771. Retrieved from https://agupubs.onlinelibrary.wiley.com/doi/abs/10.1029/2018GL081669 doi: https://doi.org/10.1029/2018GL081669

Ma, W., Wang, H., Chen, G., Qian, Y., Baxter, I., Huo, Y., & Seefeldt, M. W. (2023). Wintertime extreme warming events in the high arctic: Characteristics, drivers, trends, and the role of atmospheric rivers. *EGUsphere*. Retrieved from https://doi.org/10.5194/egusphere-2023-2018 (Preprint) doi: 10.5194/egusphere-2023-2018

Maclennan, M. L., Lenaerts, J. T. M., Shields, C., & Wille, J. D. (2022a). Contribution of atmospheric rivers to antarctic precipitation. *Geophysical Research Letters*, *49*(18), e2022GL100585. Retrieved from https://agupubs.onlinelibrary.wiley.com/doi/abs/10.1029/2022GL100585 (e2022GL100585 2022GL100585) doi: https://doi.org/10.1029/2022GL100585

Maclennan, M. L., Lenaerts, J. T. M., Shields, C., & Wille, J. D. (2022b). Contribution of atmospheric rivers to antarctic precipitation. *Geophysical Research Letters*, *49*(18). Retrieved 2024-04-16, from https://onlinelibrary.wiley.com/doi/abs/10.1029/2022GL100585 doi: 10.1029/2022GL100585

Massoud, E., Espinoza, V., Guan, B., & Waliser, D. (2019). Global climate model ensemble approaches for future projections of atmospheric rivers. *Earth's Future*, *7*(10), 1136-1151. Retrieved from https://agupubs.onlinelibrary.wiley.com/doi/abs/10.1029/2019EF001249 doi: https://doi.org/10.1029/2019EF001249

Massoud, E., Massoud, T., Guan, B., Sengupta, A., Espinoza, V., De Luna, M., ... Waliser, D. (2020). Atmospheric rivers and precipitation in the middle east and north africa (mena). *Water*, *12*(10). Retrieved from https://www.mdpi.com/2073-4441/12/10/2863 doi: 10.3390/w12102863

Mattingly, K. S., Mote, T. L., & Fettweis, X. (2018). Atmospheric river impacts on greenland ice sheet surface mass balance. *Journal of Geophysical Research: Atmospheres*, *123*(16), 8538-8560. Retrieved from https://agupubs.onlinelibrary.wiley.com/doi/abs/10.1029/2018JD028714 doi: https://doi.org/10.1029/2018JD028714

Murphy, J. M., Garcia, S., Piston, A., Moss, J. H., Howard, K., Fergusson, E. A., ... others (2022). Coastal surveys in alaska and their application to salmon run-size and harvest forecasts. *North Pacific Anadromous Fish Commission Technical Report*(18).

Nash, D., Rutz, J. J., & Jacobs, A. (2024). Atmospheric rivers in southeast alaska: Meteorological conditions associated with extreme precipitation. *Journal of Geophysical Research: Atmospheres*, *129*(4), e2023JD039294. Retrieved from https://agupubs.onlinelibrary.wiley.com/doi/abs/10.1029/2023JD039294 (e2023JD039294 2023JD039294) doi: https://doi.org/10.1029/2023JD039294

Neiman, P. J., Ralph, F. M., Wick, G. A., Kuo, Y.-H., Wee, T.-K., Ma, Z., ... Dettinger, M. D. (2008). Diagnosis of an intense atmospheric river impacting the pacific northwest: Storm summary and offshore vertical structure observed with cosmic satellite retrievals. *Monthly Weather Review*, *136*(11), 4398 - 4420. Retrieved from https://journals.ametsoc.org/view/journals/mwre/136/11/2008mwr2550.1.xml doi: 10.1175/2008MWR2550.1

Paily, P., Macagno, E., & Kennedy, J. (1974, 3). Winter-regime surface heat loss from heated streams. research report. *US Office of Scientific and Technical Information*. Retrieved from https://www.osti.gov/biblio/7179276

Paul J., N., Lawrence J., S., F. Martin, R., Mimi, H., & Gary A., W. (2011). Flooding in western washington: The connection to atmospheric rivers. *Journal of Hydrometeorology*, *12*(6), 1337 - 1358. Retrieved from https://journals.ametsoc.org/view/journals/hydr/12/6/2011jhm1358_1.xml doi: 10.1175/2011JHM1358.1

Prowse, T., Bonsal, B., Duguay, C., & Lacroix, M. (2007). River-ice break-up/freeze-up: a review of climatic drivers, historical trends and future predictions. *Annals of Glaciology*, *46*, 443–451. doi: 10.3189/172756407782871431

Prowse, T. D., & Beltaos, S. (2002). Climatic control of river-ice hydrology: a review. *Hydrological Processes*, *16*(4), 805-822. Retrieved from https://onlinelibrary.wiley.com/doi/abs/10.1002/hyp.369 doi: https://doi.org/10.1002/hyp.369

Ralph, F. M., Neiman, P. J., Wick, G. A., Gutman, S. I., Dettinger, M. D., Cayan, D. R., & White, A. B. (2006). Flooding on california's russian river: Role of atmospheric rivers. *Geophysical Research Letters*, *33*(13). Retrieved from https://agupubs.onlinelibrary.wiley.com/doi/abs/10.1029/2006GL026689 doi: https://doi.org/10.1029/2006GL026689

Rey, D., & Neuhauser, M. (2011). Wilcoxon-signed-rank test. In M. Lovric (Ed.), *International encyclopedia of statistical science* (pp. 1658–1659). Berlin, Heidelberg: Springer Berlin Heidelberg. Retrieved from https://doi.org/10.1007/978-3-642-04898-2_616 doi: 10.1007/978-3-642-04898-2_616

Saavedra, F., Cortés, G., Viale, M., Margulis, S., & McPhee, J. (2020). Atmospheric rivers contribution to the snow accumulation over the southern andes (26.5° s–37.5° s). *Frontiers in Earth Science*, *8*. Retrieved from https://www.frontiersin.org/articles/10.3389/feart.2020.00261 doi: 10.3389/feart.2020.00261

Saha, S., Moorthi, S., Pan, H.-L., Wu, X., Wang, J., Nadiga, S., ... Goldberg, M. (2010). The ncep climate forecast system reanalysis. *Bulletin of the American Meteorological Society*, *91*(8), 1015 - 1058. Retrieved from https://journals.ametsoc.org/view/journals/bams/91/8/2010bams3001_1.xml doi: 10.1175/2010BAMS3001.1

Shapiro, S. S., & Wilk, M. B. (1965). An analysis of variance test for normality (complete samples). *Biometrika*, *52*(3-4), 591–611.

Shen, H. T. (2010). Mathematical modeling of river ice processes. *Cold Regions Science and Technology*, *62*(1), 3-13. Retrieved from https://www.sciencedirect.com/science/article/pii/S0165232X10000339 doi: https://doi.org/10.1016/j.coldregions.2010.02.007

Thornton, M., Shrestha, R., Wei, Y., Thornton, P., Kao, S.-C., & Wilson, B. (2022). *Daymet: Annual climate summaries on a 1-km grid for north america, version 4 r1.* ORNL Distributed Active Archive Center. Retrieved from https://daac.ornl.gov/cgi-bin/dsviewer.pl?ds_id=2130 doi: 10.3334/ORNLDAAC/2130

Thornton, P. E., Shrestha, R., Thornton, M., Kao, S.-C., Wei, Y., & Wilson, B. E. (2021, 7 23). Gridded daily weather data for north america with comprehensive uncertainty quantification. *Scientific Data*, *8*(1), 190. Retrieved from https://doi.org/10.1038/s41597-021-00973-0 doi: 10.1038/s41597-021-00973-0

Viale, M., Valenzuela, R., Garreaud, R. D., & Ralph, F. M. (2018). Impacts of atmospheric rivers on precipitation in southern south america. *Journal of Hydrometeorology*, *19*(10), 1671 - 1687. Retrieved from https://journals.ametsoc.org/view/journals/hydr/19/10/jhm-d-18-0006_1.xml doi: 10.1175/JHM-D-18-0006.1

Wang, Z., Ding, Q., Wu, R., Ballinger, T. J., Guan, B., Bozkurt, D., ... Chen,

Z. (2024, June 29). Role of atmospheric rivers in shaping long term arctic moisture variability. *Nature Communications*, *15*(1), 5505. Retrieved from https://doi.org/10.1038/s41467-024-49857-y doi: 10.1038/s41467-024-49857-y

Wille, J. D., Favier, V., Gorodetskaya, I. V., Agosta, C., Kittel, C., Beeman, J. C., . . . Codron, F. (2021). Antarctic atmospheric river climatology and precipitation impacts. *Journal of Geophysical Research: Atmospheres*, *126*(8), e2020JD033788. Retrieved from https://agupubs.onlinelibrary.wiley.com/doi/abs/10.1029/2020JD033788 (e2020JD033788 2020JD033788) doi: https://doi.org/10.1029/2020JD033788

Zhang, P., Chen, G., Ting, M., Ruby Leung, L., Guan, B., & Li, L. (2023, March). More frequent atmospheric rivers slow the seasonal recovery of arctic sea ice. *Nature Climate Change*, *13*(3), 266–273. Retrieved from https://doi.org/10.1038/s41558-023-01599-3 doi: 10.1038/s41558-023-01599-3

Zhu, Y., & Newell, R. E. (1998). A proposed algorithm for moisture fluxes from atmospheric rivers. *Monthly Weather Review*, *126*(3), 725 - 735. Retrieved from https://journals.ametsoc.org/view/journals/mwre/126/3/1520-0493_1998_126_0725_apafmf_2.0.co_2.xml doi: 10.1175/1520-0493(1998)126⟨0725:APAFMF⟩2.0.CO;2

Appendix A.

Table 1. Table showing the Pearson correlation coefficients between the total thermal energy exchange (Q) as derived by Equation 3, assuming an exponential temporal bias (Equation 2), and the day of the year the breakup occured (DOY), by location. The optimal center placement of the temporal bias (month-day) is also provided [r_p|center date of bias]

Location	**Total Precipitation**	**Precipitation from ARs**	**Precipitation not from ARs**
Akiak Kuskokwim River	−0.78|11-12	−0.78|2-5	−0.80|1-15
Allakaket Koyukuk River	−0.81|12-10	−0.69|10-23	−0.80|12-3
Ambler Kobuk River	−0.84|2-5	−0.67|2-5	−0.83|2-12
Aniak Kuskokwim River	−0.80|11-19	−0.81|1-29	−0.77|11-12
Bethel Kuskokwim River	−0.72|12-3	−0.75|2-5	−0.73|12-10
Bettles Koyukuk River	−0.79|2-19	−0.70|10-23	−0.81|2-12
Circle Yukon River	−0.75|2-5	−0.76|1-22	−0.74|2-12
Crooked Creek Kuskokwim River	−0.84|11-26	−0.76|2-5	−0.80|11-26
Dawson Yukon River	−0.77|10-23	−0.67|1-22	−0.75|10-23
Eagle Yukon River	−0.77|10-23	−0.79|1-22	−0.76|1-29
Emmonak Yukon River	−0.76|2-5	−0.76|1-29	−0.71|4-16
Fort Yukon Yukon River	−0.72|10-23	−0.59|2-5	−0.72|10-23
Galena Yukon River	−0.79|11-19	−0.75|1-15	−0.80|4-16
Holy Cross Yukon River	−0.75|1-8	−0.77|1-8	−0.72|1-8
Hughes Koyukuk River	−0.81|1-1	−0.78|1-15	−0.78|4-2
Kaltag Yukon River	−0.84|12-3	−0.77|12-3	−0.86|1-15
Kobuk Kobuk River	−0.81|1-8	−0.62|4-16	−0.81|1-8
McGrath Kuskokwim River	−0.81|3-26	−0.81|2-5	−0.82|4-9
Mountain Village Yukon River	−0.72|1-29	−0.76|2-5	−0.69|2-19
Nenana Tanana River	−0.71|1-1	−0.73|2-5	−0.72|1-1
Nikolai Kuskokwim River	−0.75|2-12	−0.70|2-5	−0.74|1-15
Red Devil Kuskokwim River	−0.79|12-3	−0.80|2-5	−0.78|12-3
Ruby Yukon River	−0.83|4-9	−0.78|1-15	−0.86|4-16
Russian Mission Yukon River	−0.71|11-26	−0.72|12-10	−0.68|12-3
Tanana Yukon River	−0.76|1-22	−0.70|2-5	−0.77|11-26

Influence of Atmospheric Rivers on Alaskan River Ice

Russ Limber[1,2], Elias C. Massoud[2], Bin Guan[3,4], Forrest M. Hoffman[2], Jitendra Kumar[2]

[1]The University of Tennessee, Knoxville, Knoxville, TN, USA
[2]Oak Ridge National Laboratory, Oak Ridge, TN, USA
[3]Joint Institute for Regional Earth System Science and Engineering, University of California, Los Angeles, CA, USA
[4]Jet Propulsion Laboratory, California Institute of Technology, Pasadena, CA, USA

Key Points:

- Interannually, atmospheric rivers (ARs) can lead to a week-long persistent increase in daily air temperatures over Interior Alaska (AK)
- In AK, ARs account for 36% of annual precipitation, 57% of extreme precipitation and explain 48% of interannual variability of precipitation
- AR events during the coldest months delay the annual breakup date of river ice, while ARs closer to the breakup date have less impact

Corresponding author: Russ Limber, `r62@ornl.gov`

Abstract

Atmospheric rivers (ARs) transport vast amounts of moisture from low to high latitude regions. One region particularly impacted by ARs is Interior Alaska (AK). We analyze the impact of ARs on the annual river ice breakup date for 25 locations in AK. We investigate the AR-driven rise in local air temperatures and explore the relationship between ARs and precipitation, including extremes and interannual variability. We found that AR events lead to an increase in local air temperatures for up to one week (by ≈ 1 °C). Interannually, ARs account for 36% of total precipitation, explain 48% of precipitation variability, and make up 57% of extreme precipitation events. By estimating the heat transfer between winter precipitation and the river ice surface, we conclude that increased precipitation during the coldest period of the year delays river ice breakup dates, while precipitation occurring close to the breakup date has little impact on breakup timing.

Plain language summary

Atmospheric rivers (ARs) are large storm systems originating in tropical regions capable of depositing large amounts of precipitation in high latitude regions. Using river ice breakup data recorded throughout Interior Alaska (AK) we set out to explore the relationship between ARs and annual river ice breakup timing from 1980 to 2023. We found that daily air temperature increases can last up to one week after an AR event. Interannually, ARs account for 36% of total precipitation, explain 48% of the variability of precipitation, and make up 57% of extreme precipitation events. We then approximated the total heat transfer between precipitation and the river ice surface. We used the mass and temperature of precipitation accumulated on the river ice surface to approximate thermal energy exchange. The magnitude of energy exchange was then correlated to river ice breakup timing. We found that greater amounts of precipitation from both AR and non-AR induced precipitation, occuring relatively close to river ice breakup dates, have little correlation to the breakup date. However, increased precipitation during the coldest period of the year (typically late December to early February) is strongly inversely correlated with river ice breakup timing and seems to delay the breakup date.

1 Introduction

Atmospheric rivers (ARs) are narrow corridors of intense water vapor that significantly influence hydrologic events, transporting most of the water vapor outside of the Tropics (American Meteorological Society, 2024). It is estimated that ARs are responsible for as much as 90% of poleward water vapor transport at midlatitudes (Zhu & Newell, 1998). ARs contribute to extreme precipitation events across various regions worldwide (Espinoza et al., 2018; Massoud et al., 2019), including Western North America (Dettinger et al., 2004; Neiman et al., 2008; Guan et al., 2010; Paul J. et al., 2011; Ralph et al., 2006; F. Martin et al., 2019; Dettinger et al., 2011) Europe (Lavers et al., 2013; Harald & Andreas, 2013), the Middle East (Massoud et al., 2020; Lashkari & Esfandiari, 2020; Esfandiari & Shakiba, 2024), and Western South America (Viale et al., 2018). In recent years, the impacts of ARs on the cryosphere such as Greenland (Mattingly et al., 2018) and Antarctica (Gorodetskaya et al., 2014; Wille et al., 2021; Maclennan et al., 2022a), have been more extensively analyzed. In addition, a growing number of works investigating the relationship between ARs and high latitude regions have been undertaken (Hegyi & Taylor, 2018; Wang et al., 2024). Evidence shows that between 1981 and 2020, higher atmospheric moisture content was significantly correlated with lower sea ice coverage over almost the entire Arctic Ocean (Li et al., 2022). For those same years, another analysis found that 100% of extreme temperature events in the Arctic (above 0 °C) coincide with the presence of ARs (Ma et al., 2023). Analyses have noted a relationship between frequent AR activity and sea ice loss, caused by increased rainfall from moisture originating in lower latitudes (Zhang et al., 2023; Maclennan et al., 2022b). However, Arctic systems are complicated, as the intense moisture transport within ARs can also result in heavy snowfall events, thus contributing to the accumulation of snowpack, especially in mountainous regions (Saavedra et al., 2020; Guan et al., 2010). Under the right conditions, this relationship has been found to actually increase the mass balance of glaciers. Little et al. (2019) found ARs to be the primary drivers of both highest ablation and snowfall events, substantially impacting glacier mass balance at Brewster Glacier in New Zealand. Understanding the role of ARs in the cryosphere is essential for assessing their broader impact on regional water resources and glacier dynamics in a changing climate.

While a number of works have explored the relationship between ARs and sea ice, glaciers, and ice sheets, to our knowledge there has been no study that investigates the relationship between ARs and Arctic river ice. Past studies have used physics based processes to model the annual breakup timing and conditions of Arctic river ice (Paily et al., 1974; G. Ashton, 1986; T. Prowse et al., 2007; Jasek, 1998; Shen, 2010). Through such studies, it is recognized that an increase in precipitation leads to an increase in streamflow, altering the hydraulics associated with river ice breakup, and potentially accelerating mechanical breakup events (G. Ashton, 1986). It has also been proposed that increased snow pack as a result of increased precipitation contributes to breakup severity (T. D. Prowse & Beltaos, 2002). Using breakup records throughout Interior Alaska (AK) from the Alaska-Pacific River Forecast Center Database (the same breakup records used in this analysis) Bieniek et al. (2011) determined that winter precipitation plays a relatively minor role in impacting the breakup timing of river ice and if anything accelerates the breakup timing as a result of increased streamflow. They also report that increased storm activity in the spring leads to increased surface air temperature, leading to earlier breakup dates (Bieniek et al., 2011). However, their analysis used only 4 sites (as opposed to the 25 used in this analysis) and aggregated precipitation seasonally, without accounting for the interaction between winter precipitation and temperature that occurs at a finer temporal resolution.

Our analysis aims to answer the following questions: 1.) Since ARs have been known to impact Arctic systems by increasing temperatures, is there a change in air temperature in different regions of AK corresponding to the presence of ARs? 2.) How do ARs contribute to precipitation throughout AK, considering how ARs impact total annual precipitation, interannual variability, and extreme events? 3.) How do ARs impact the timing of river ice breakup, does the presence of ARs accelerate or delay the timing of river ice breakup?

2 Data

2.1 Atmospheric Rivers Catalog

Similar to previous studies, we define ARs using integrated vapor transport (IVT) constructed from 6-hourly values of 3-D wind and water vapor at eight pressure levels between 300 and 1,000 mb from the National Center for Environmental Protection (NCEP) reanalysis data product (Kalnay et al., 1996). AR detection is based on version 3 of the tARget algorithm (Guan & Waliser, 2019; Guan, 2022). The IVT values are calculated at the original resolution from the NCEP meteorological inputs (Saha et al., 2010). Guan and Waliser (2015) developed a global AR detection algorithm, which was updated and validated later with dropsonde data (Bin et al., 2018). This algorithm is employed in our study, which is based on a combination of IVT magnitude, direction, and geometry characteristics, to objectively identify ARs. Contiguous regions of enhanced IVT transport are first identified from magnitude thresholding (i.e. grid cells above the seasonally and locally dependent 85^{th} percentile, or $100\frac{\text{kg}}{\text{m}*\text{s}}$, whichever is greater) and further filtered using directional and geometry criteria requirements. Although the $100\frac{\text{kg}}{\text{m}*\text{s}}$ threshold is applied globally, it is intended for dry (including polar) regions since in other regions the 85^{th} percentile is already larger than $100\frac{\text{kg}}{\text{m}*\text{s}}$. The detection algorithm was applied to

NCEP reanalysis data at its native resolution of 2.5°. This detection algorithm had over 90% agreement in detecting AR landfall dates when compared with other AR detection methods for Western North America (Neiman et al., 2008), the United Kingdom (Lavers et al., 2011), and East Antarctica (Gorodetskaya et al., 2014).

2.2 Daymet Daily Surface Weather and Climatological Summaries

Daily minimum ($T_{\min}$) and maximum ($T_{\max}$) temperatures and precipitation data were obtained from Daymet (M. Thornton et al., 2022). Daymet provides continuous and gridded estimates of daily weather at 1km × 1km resolution. Daymet precipitation, $T_{\min}$ and $T_{\max}$, were selected in this analysis due to their strong agreement with NCEP temperature time series for our region of interest (Figure 1C). Daymet is derived by interpolating and extrapolating from in situ instruments and meteorological stations, and represents a robust dataset for precipitation and temperature predictions across North America (P. E. Thornton et al., 2021). This dataset has been a standard for validation among several analyses related to arctic regions (Diro & Sushama, 2019; Akinsanola et al., 2024). Figure 1 (A, B) show the annual mean precipitation and temperature for the year 2021 across Alaska. For one of the study locations, Crooked Creek at the Kuskokwim River, Figure 1 (C) shows the time series of precipitation, temperature and AR events for the year 2021.

2.3 River ice breakup observations

Observations for river ice breakup dates were obtained from the Alaska-Pacific River Forecast Center database. While exact coordinates were unavailable, location coordinates were estimated based on proximity to weather stations and airports, to maintain spatial consistency with inputs used in Daymet's meteorological models. We identified 25 locations (shown in Figure 1 (A, B)) in the database that had at least 35 breakup records between 1980 and 2023 (the current temporal availability of Daymet), although breakup records go as far back as 1896 for some locations. The 35 breakup records threshold was used because it allowed for the greatest number of locations with the most complete time series necessary for statistical analysis. There is always one breakup date per year, but not every year had a recorded date, so some years are represented as empty values in the dataset. On average, recorded breakup dates range from mid-March to late-June This dataset has been used in several other studies such as (Murphy et al., 2022; Brown et al., 2018; Bieniek et al., 2011). As an example, the breakup date for Crooked Creek at the Kuskokwim River in 2021 occurred in early-May and is depicted in Figure 1 (C) with a vertical purple dashed line.

3 Methods

To assess the influence of ARs on local temperature, we analyze the relationship between the presence of an AR and the temperature change at a specific location. The presence of an AR is represented numerically as a binary value indicating whether or not an AR is active on a particular date. We then estimate how many days this change in temperature persists. To do this, we conducted a pairwise t-test using a varying temporal window. In other words, for each AR occurrence in the dataset, a pre–AR time window and post–AR time window each equal to n days in length was created before and after the AR event date, respectively, whereby: $n \in \{1, 2, 3, \ldots, 14\}$. For values of n greater than one day the mean was calculated within each time window for $T_{\min}$ and $T_{\max}$. These averaged temperatures were then calculated over all locations. Mean temperature pairs were assessed using a one tailed pairwise t-test to check whether ARs increased the local temperature over period of time n ($\alpha = 0.05$). For example, if $n = 3$ assessing $T_{\min}$, then the mean of $T_{\min}$ three days prior to each AR event will be compared to the mean of $T_{\min}$ for the three days post each AR event.

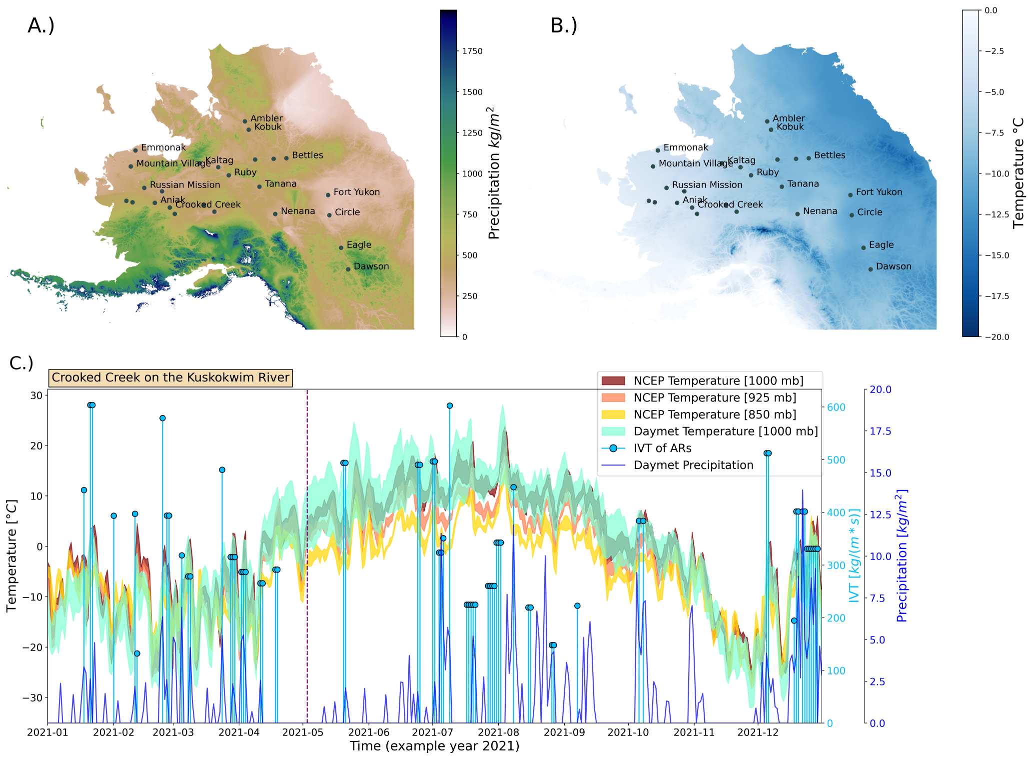

Figure 1. (A): map shows annual total precipitation for the year 2021. (B): map of average daily temperature for 2021. (C): One of the 25 locations (Crooked Creek on the Kuskokwim River) for the year 2021. Yellow, orange, red represent the temperature profiles (fill plot of T_{min} - T_{max}) from NCEP temperature data at 850, 925 and 1000mb respectively. Light green represents the Daymet temperature profile. Dark blue line shows precipitation from Daymet ($\frac{\text{kg}}{\text{m}^2}$) relative to the secondary y-axis in dark blue on the right. The light blue stem plots depict the IVT of AR events ($\frac{\text{kg}}{\text{m}*\text{s}}$) relative to the secondary y-axis in light blue on the right. The vertical purple dashed line shows the breakup date for the Kuskokwim River in 2021 for Crooked Creek.

We explored AR contribution to precipitation by seperating precipitation events occuring on days with an active AR. We then used the Wilcoxon rank-sum test (Rey & Neuhauser, 2011) to test the hypothesis that AR events tend to produce more precipitation than other precipitation events. We opted to use a non-parametric test (Wilcoxon rank-sum test) because the distributions of precipitation were shown to not be normal after log transformation using the Shapiro-Wilks test (Shapiro & Wilk, 1965). We also estimated the interannual variability of precipitation associated with ARs by conducting a univariate ordinary least squares regression (OLS). For extremes, we extracted the top 5% of precipitation events and determined what fraction of those events occured on days with an active AR event.

To determine the impact that ARs have on river ice breakup timing, we estimate the heat transfer between the river ice and the precipitation accumulating on the surface. Assuming presence of a frozen layer of ice on the river surface, we estimate the sensible heat transfer between the river surface and incoming precipitation using Equation 1. Latent heat transfer fluxes were assumed to be relatively small and thus ignored in our simplified heat transfer calculations. The specific heat of precipitation in Equation 1 is represented as either water or liquid as determined by air temperature. Given that Alaska is at a high latitude with heat transfer calculated during the coldest period of the year, it can be assumed that in most cases the precipitation is in the form of snow.

$$q_t = \rho \cdot m \cdot \Delta T \tag{1}$$

where q_t is heat flux ($\frac{\mathrm{J}}{\mathrm{m}^2}$) at a given day t; ρ the specific heat of the precipitation (assumed to be either water or snow depending on the temperature) ($\frac{\mathrm{J}}{\mathrm{kg}^\circ\mathrm{C}}$); ΔT is the difference between the temperature of the precipitation which is approximated using T_{min} as a proxy, and the river ice surface which is assumed to be at 0 °C; m the mass of the precipitation per unit area ($\frac{\mathrm{kg}}{\mathrm{m}^2}$).

Heat transfer fluxes were calculated as a daily series for a period of six months prior to the breakup date. Time of occurrence and thermal conditions associated with precipitation events during winter and spring have differential impacts to reinforce versus weaken the river ice layer and thus the date of the breakup. We fit a temporal bias function (Equation 2), a double exponential function, applied to the heat transfer equation to assess the days of the year when precipitation events were more impactful on breakup timing. The bias function is a symmetric unimodal exponential function to help identify the most influencial precipitation time period determining the annual time of river ice breakup. This bias function was fit individually for each of the study locations.

$$f(t;\gamma,\kappa,DOY,c) = \begin{cases} \frac{e^{-\gamma\cdot(-t-DOY)}-1}{\kappa} & \text{if } t < c \\ \frac{e^{-\gamma\cdot(t-DOY)}-1}{\kappa} & \text{if } t \geq c \end{cases} \tag{2}$$

where γ is a scale parameter impacting the width of the exponential function; t is time in days; DOY is the Gregorian day of year that the breakup date occurred; c is a location parameter dictating the center placement of the function; κ is a normalizing constant. Finally, Equation 3 solves for $Q_{\text{year, location}}$, the total thermal energy exchange for a given location, for a given breakup year. Equation 3 is tuned over the entire hyperparameter search space for each location and each breakup year, optimized by selecting the parameter values that produce the Pearson correlation coefficient with the greatest absolute value. Here i is the starting day of the time series approximately six months prior to the breakup date.

$$Q_{\text{year, location}} = \sum_{t=i}^{t=DOY} f(t;\gamma,\kappa,DOY,c) \cdot q_t \tag{3}$$

4 Results

4.1 Atmospheric rivers impact on temperature

We applied the pairwise t-test comparing pre–AR and post–AR time windows of length n at all locations. Figures 2A and 2B show the change in p-values for each value of n where the dashed lines represent the mean p-value across the study locations and the filled color curved signifies the interquartile range (IQR). Figure 2C and 2D shows the mean increase in temperature from the pre–AR time window to the post–AR time window for varying time window sizes n. Analysis shows an increase in air temperature during the period following an AR event, with mean temperature increases higher for $T_{\min}$ compared to $T_{\max}$, with the difference receding over longer time windows. On average, the temperature differences were statistically significant for $T_{\min}$ (based on an $\alpha = 0.05$) for temporal windows up to 10 days after an AR event. For temporal windows up to 7 days, statistical significance was true for all locations within the study as represented by the Figure 2A fill plot. The increase in daily minimum temperature can be as high as 1.5 °C ($n = 2$) (Figure 2C). For $T_{\max}$, the differences were statistically significant for up to 6 days after an AR event on average (Figure 2B) with an increase as high as 0.75 °C ($n = 3, 4$) (Figure 2D). These statistically significant temperature increases following AR events were true at all locations in our study for $n = 2, 3, 4$ as shown in Figure 2B fill plot.

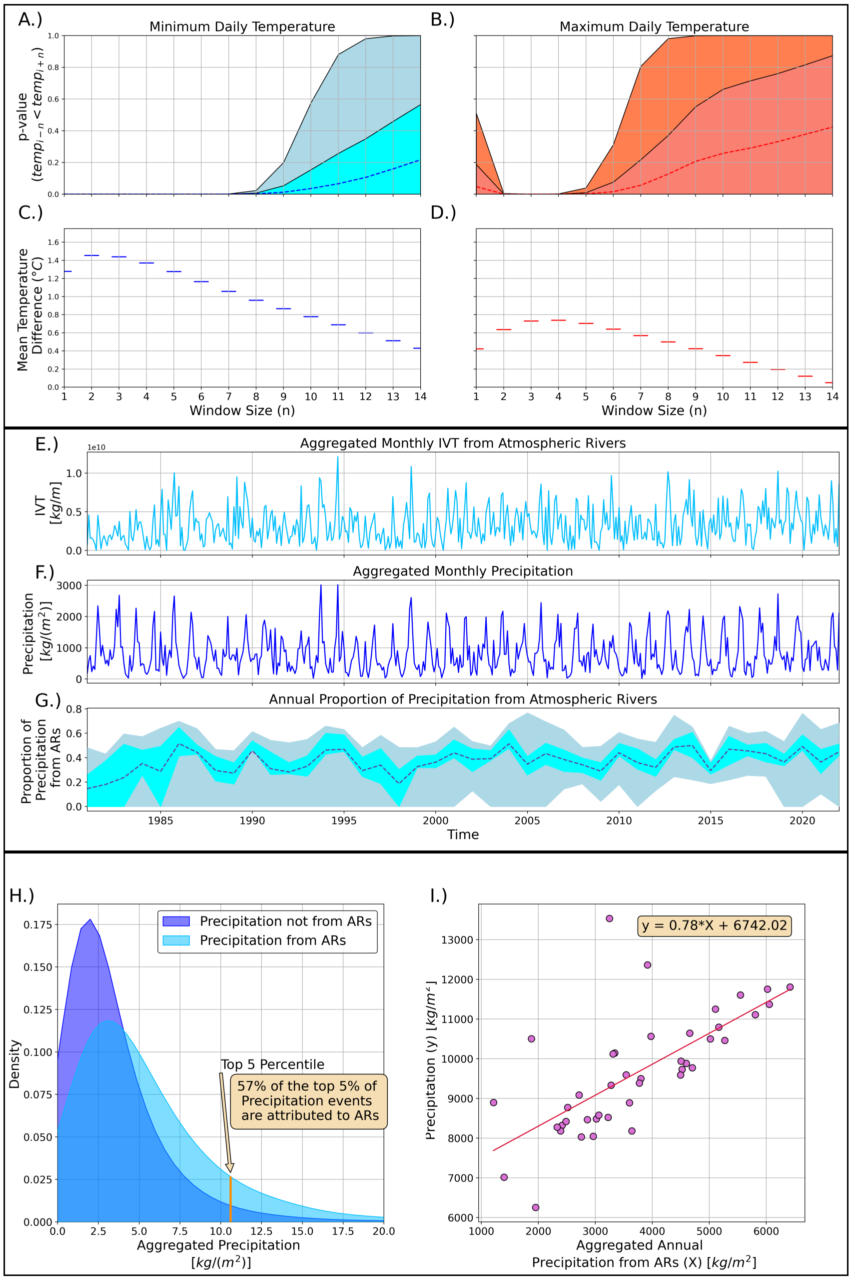

Figure 2. (A and B): p-values from the paired t-test given time window size (n) surrounding the AR event date (A: $T_{\min}$; B: $T_{\max}$). Dashed lines represent the mean, while the filled color curves show interquartile range (25th and 75th percentile); (C and D): mean increase in temperature (°C) accompanying each AR, calculated between the pre–AR time window and the post–AR time window (C: $T_{\min}$; D: $T_{\max}$). (E): time series of IVT $\frac{\text{kg}}{\text{m}}$ aggregated monthly over all locations. (F): time series of total precipitation $\frac{\text{kg}}{\text{m}^2}$ aggregated monthly over all study locations. (G): proportion of precipitation accounted for by ARs on an annual basis. (H): kernel density plots showing the distribution of local precipitation (dark blue) and precipitation from ARs (light blue). (I): ordinary least squares regression plot using total annual precipitation from ARs, to predict total annual precipitation.

4.2 Atmospheric rivers impact on precipitation

Figures 2E and 2F show the monthly IVT from AR events and monthly total precipitation through the span of the data record, aggregated over all locations, respectively. Figure 2G shows the proportion of total annual precipitation occuring on days with active ARs over time, where light blue depicts the IQR of proportions and blue-grey represents proportions outside of the IQR, across all 25 locations. The dashed line represents the mean proportion. ARs tend to account for 36% of precipitation on average (Figure 2G), with a high degree of variability across years and locations. In 2005 and 2020 for example, nearly 80% of the total precipitation at some locations occured on days with active AR events. The results from the Wilcoxon rank-sum test show that precipitation during active ARs tends to be greater in magnitude than non-AR precipitation (test statistic = -83.85; p-value ≈ 0.0). In addition, we found that of the top 5% of precipitation events by total rainfall, 57% occured during active ARs (Figure 2H). Correlating total precipitation from AR days, to total annual precipitation using a univariate OLS, we find that the coefficient of determination (R^2) is equal to 0.48 (Figure 2I). This indicates that ARs explain about 48% of interannual variability in precipitation, across all 25 locations.

4.3 Transfer of energy based on Precipitation

To estimate the impact of precipitation on river ice breakup dates, we use Equation 3 to approximate the heat transfer between precipitation and the river ice surface. Equation 3 was solved using a double exponential bias function to temporally-weigh events of higher influence (Figures 3A, 3B, 3C), and using uniform weights as baseline for comparison (Figures 3D, 3E, 3F). When using a temporal bias function, the relationship between summated heat transfer due to precipitation and time of river ice breakup were identified with strong correlation (Pearson correlation coefficient (r_p) = -0.84 and a Spearman correlation coefficient (r_s) = -0.80 at Crooked Creek on the Kuskokwim river (Figure 3A)). In contrast, very weak correlations were identified when fitting the relationship using temporally uniform weights (Figure 3B), thus highlighting the need for a temporal bias function. We tuned three different cases for Equation 1 whereby the mass of precipitation could be provided by: total precipitation, precipitation from ARs or precipitation not from ARs. This exercise allows us to determine whether or not that aggregated energy accelerates or decelerates the breakup of river ice. We find that there is a strong negative correlation between the heat transfer and the DOY on which the river ice breakup occurs (Figure 3A). In this context, negative values along the y-axis of Figures 3A and 3D are interpreted as a negative heat exchange, suggesting a net cooling effect on the river ice surface as the precipitation below freezing are accumulated on the river ice surface. The peak of the temporally-weighted bias curve is typically located during the coldest period of the year, typically betweeen late November and early February (Figure 3C). In other words, the presence of high magnitude precipitation events, occuring on colder days of the year, show a strong inverse correlation to the time of breakup. For example, referring to Figure 3A, Crooked Creek on the Kuskokwim River has a clear negative trend, whereby the cooling effect of precipitation on the river ice surface delays the DOY of the breakup. The frequency of AR events that occurred six months prior to the breakup date alone is an insufficient predictor (Figures 3B, 3E) of the breakup date.

While Figure 3 focuses on a single selected site, Table 1 shows the Pearson correlation after tuning parameters c and γ are optimized and applied to Equation 3 individually at each location. Table 1 also shows the center of the bias curve c (month-day) that was selected for, at each location, given the summand for precipitation used in Equation 3 (ie. Total Precipitation, Precipitation from ARs, Precipitation not from ARs; mulitplied to the temporal bias).

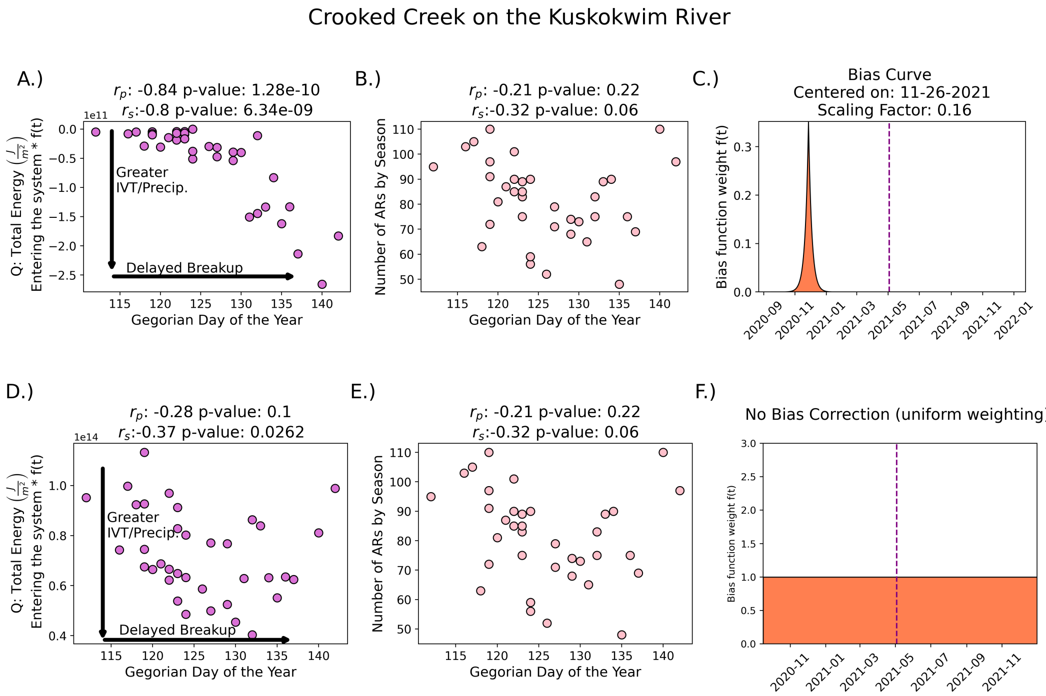

Figure 3. top row: (A): scatter plot between thermal energy transfer for all precipitation events and DOY (the Gregorian day of year that the breakup date occurred); (B): scatter plot of the number of ARs that occured in the six months prior to the breakup date and DOY; (C): temporal bias curve for the year 2021 with the breakup date represented by the vertical dashed line. bottom row: same as the top row except depicting the results when a temporal bias is not utilized.

5 Conclusion and Discussion

This study investigated the impact atmospheric rivers (ARs) and non-AR related precipitation events have on the timing of river ice breakup across 25 sites in Alaska. We explored the impact of ARs on local temperature increases throughout the study domain; the contribution of ARs to precipitation events, including variability and extremes; and determined the impact of ARs and non-AR precipitation events on the DOY on which the ice on the surface of Alaskan rivers eventually breaks.

We found that ARs generally lead to up to a week-long persistent increase in daily temperature (minimum and maximum) across Alaska, with temperatures rising by as much as 1.5 °C for $T_{\min}$ and 0.75 °C for $T_{\max}$. These findings are consistent with many past studies that have shown that warm moisture and an increase in heat flux brought on by ARs can warm the cryosphere (Wille et al., 2021; Ma et al., 2023; Li et al., 2022; Zhang et al., 2023). Our analysis also shows that ARs account for a significant portion of total annual precipitation in Alaska, contributing to 36% of total precipitation by volume on average. ARs also explain 48% of interannual variability and lead to 57% of extreme precipitation events (precipitation events within the top 5% of deposition). These results are consistent with past works, such as Nash et al. (2024) which showed that throughout Southeast Alaska, as few as six annual AR events can account for 68% - 91% of precipitation days. Our analysis shows evidence that intense ARs occurring during the coldest period of the year appear to delay the annual breakup date of river ice. Our results do not show that ARs are unique relative to non-AR forms of precipitation in this regard (Table 1), with no evidence that increased precipitation events of any kind closer to the breakup date accelerates the breakup date. This is likely attributed to a combination of heat transfer from precipitation, increased ice accumulation on the river ice surface and structural changes in the river ice as a result of snowfall. Increased snow accumulation increases the albedo of the river surface, as well as provides thermal insulation, mitigating the effects of temperature fluctuations during the coldest period of the year. This is consistent with the extensive analysis conducted by G. D. Ashton (2011), showing that an increase in snow accumulation on the river ice surface for locations across Alaska (many of the same locations used in this analysis) can lead to an increase in river ice thickness, thus reinforcing the river ice structurally. This phenomenon is apparent to a point at which the efficacy begins to diminish. It should be noted that a limitation of our analysis is the assumption that the river ice surface temperature is held constant at 0 °C and that air temperature is a reasonable proxy for incoming precipitation. We were unable to find a complete dataset on river ice surface temperatures for the locations and time period of our study. Thus, we assume that the mass of liquid, snow or ice deposited on the river surface, times its temperature and specific heat, will be sufficient to approximate the heat exchanged in the system.

Understanding the influence of ARs and other high precipitation events on the timing of river ice breakup in Alaska is crucial for predicting and managing the impacts of climate change in the region, especially since studies have shown that AR frequency and intensity in this region are expected to increase in a warmer world (Espinoza et al., 2018; Massoud et al., 2019). The findings of our analysis suggests that ARs have significant influence on the climate and terrestrial hydrology across Alaska, affecting temperature, precipitation, and river ice dynamics. Further research in this area could help improve our understanding of ARs and their role in shaping the climate of high-latitude regions.

Data Availability Statement

Daily Daymet precipitation and temperature data is available through the Oak Ridge National Laboratory Distributed Active Archive at `https://daymet.ornl.gov/single-pixel/`. River ice breakup records are maintained by the Alaska-Pacific River Forecast Center at `https://www.weather.gov/aprfc/breakupMap`. The AR database (`https://doi.org/10.25346/S6/YO15ON`) is available via the Global Atmospheric Rivers Dataverse at `https://dataverse.ucla.edu/dataverse/ar`. NCEP-NCAR Reanalysis 1 data was obtained from the NOAA Physical Sciences Laboratory, Boulder, Colorado, USA, `https://psl.noaa.gov/data/index.html`. All of the codes needed to run the analysis and everything required to reproduce this work are available on GitHub: `https://github.com/Russtyhub/River_Ice_AR_Analysis.git`.

Acknowledgments

This work was supported by the U.S. Department of Energy, Office of Science, Biological and Environmental Research (BER) Regional and Global Model Analysis (RGMA) program, as part of The Interdisciplinary Research for Arctic Coastal Environments (InteRFACE) project. Development of the AR database was supported by NASA and the California Department of Water Resources. This manuscript has been authored in part by UT-Battelle, LLC, under contract DE-AC05-00OR22725 with the US Department of Energy (DOE). The publisher acknowledges the US government license to provide public access under the DOE Public Access Plan (http://energy.gov/ downloads/doe-public-access-plan).

References

Akinsanola, A. A., Jung, C., Wang, J., & Kotamarthi, V. R. (2024). Evaluation of precipitation across the contiguous united states, alaska, and puerto rico in multi-decadal convection-permitting simulations. *Scientific Reports*, *14*(1), 1238. Retrieved from https://doi.org/10.1038/s41598-024-51714-3 doi: 10.1038/s41598-024-51714-3

American Meteorological Society. (2024). *Glossary of meteorology: Atmospheric river.* Retrieved from https://glossary.ametsoc.org/wiki/Atmospheric_river?__cf_chl_tk=LTK3vMNlWxxKfhHCGpS05IMiQaNMnEAledLyvfTD7T0-1717350416-0.0.1.1-4330 (Accessed: 2024-06-03)

Ashton, G. (1986). *River and lake ice engineering.* Water Resources Publications. Retrieved from https://books.google.com/books?id=xglYVjAsnt8C

Ashton, G. D. (2011). River and lake ice thickening, thinning, and snow ice formation. *Cold Regions Science and Technology*, *68*(1), 3-19. Retrieved from https://www.sciencedirect.com/science/article/pii/S0165232X11000875 doi: https://doi.org/10.1016/j.coldregions.2011.05.004

Bieniek, P. A., Bhatt, U. S., Rundquist, L. A., Lindsey, S. D., Zhang, X., & Thoman, R. L. (2011). Large-scale climate controls of interior alaska river ice breakup. *Journal of Climate*, *24*(1), 286 - 297. Retrieved from https://journals.ametsoc.org/view/journals/clim/24/1/2010jcli3809.1.xml doi: 10.1175/2010JCLI3809.1

Bin, G., Duane E., W., & F. Martin, R. (2018). An intercomparison between reanalysis and dropsonde observations of the total water vapor transport in individual atmospheric rivers. *Journal of Hydrometeorology*, *19*(2), 321 - 337. Retrieved from https://journals.ametsoc.org/view/journals/hydr/19/2/jhm-d-17-0114_1.xml doi: 10.1175/JHM-D-17-0114.1

Brown, D. R. N., Brinkman, T. J., Verbyla, D. L., Brown, C. L., Cold, H. S., & Hollingsworth, T. N. (2018). Changing river ice seasonality and impacts on interior alaskan communities. *Weather, Climate, and Society*, *10*(4), 625 - 640. Retrieved from https://journals.ametsoc.org/view/journals/wcas/10/4/wcas-d-17-0101_1.xml doi: 10.1175/WCAS-D-17-0101.1

Dettinger, M. D., Cayan, D. R., Meyer, M. K., & Jeton, A. E. (2004). Simulated hydrologic responses to climate variations and change in the merced, carson, and american river basins, sierra nevada, california, 1900–2099. *Climatic Change*, *62*(1), 283–317. Retrieved from https://doi.org/10.1023/B:CLIM.0000013683.13346.4f doi: 10.1023/B:CLIM.0000013683.13346.4f

Dettinger, M. D., Ralph, F. M., Das, T., Neiman, P. J., & Cayan, D. R. (2011). Atmospheric rivers, floods and the water resources of california. *Water*, *3*(2), 445–478. Retrieved from https://www.mdpi.com/2073-4441/3/2/445 doi: 10.3390/w3020445

Diro, G. T., & Sushama, L. (2019). Simulating canadian arctic climate at convection-permitting resolution. *Atmosphere*, *10*(8). Retrieved from https://www.mdpi.com/2073-4433/10/8/430 doi: 10.3390/atmos10080430

Esfandiari, N., & Shakiba, A. (2024). The extraordinary atmospheric rivers analysis over the middle east: Large-scale drivers, structure, effective sources, and precipitation characterization. *Dynamics of Atmospheres and Oceans*, *105*, 101430. Retrieved from https://www.sciencedirect.com/science/article/pii/S0377026523000817 doi: https://doi.org/10.1016/j.dynatmoce.2023.101430

Espinoza, V., Waliser, D. E., Guan, B., Lavers, D. A., & Ralph, F. M. (2018). Global analysis of climate change projection effects on atmospheric rivers. *Geophysical Research Letters*, *45*(9), 4299-4308. Retrieved from https://agupubs.onlinelibrary.wiley.com/doi/abs/10.1029/2017GL076968 doi: https://doi.org/10.1029/2017GL076968

F. Martin, R., Jonathan J., R., Jason M., C., Michael, D., Michael, A., David, R., ... Chris, S. (2019). A scale to characterize the strength and impacts of atmospheric rivers. *Bulletin of the American Meteorological Society*, *100*(2), 269 -

289. Retrieved from https://journals.ametsoc.org/view/journals/bams/100/2/bams-d-18-0023.1.xml doi: 10.1175/BAMS-D-18-0023.1

Gorodetskaya, I. V., Tsukernik, M., Claes, K., Ralph, M. F., Neff, W. D., & Van Lipzig, N. P. M. (2014). The role of atmospheric rivers in anomalous snow accumulation in east antarctica. *Geophysical Research Letters*, *41*(17), 6199-6206. Retrieved from https://agupubs.onlinelibrary.wiley.com/doi/abs/10.1002/2014GL060881 doi: https://doi.org/10.1002/2014GL060881

Guan, B. (2022). *[Data] Global Atmospheric Rivers Database, Version 3.* UCLA Dataverse. Retrieved from https://doi.org/10.25346/S6/YO15ON doi: 10.25346/S6/YO15ON

Guan, B., Molotch, N. P., Waliser, D. E., Fetzer, E. J., & Neiman, P. J. (2010). Extreme snowfall events linked to atmospheric rivers and surface air temperature via satellite measurements. *Geophysical Research Letters*, *37*(20). Retrieved from https://agupubs.onlinelibrary.wiley.com/doi/abs/10.1029/2010GL044696 doi: https://doi.org/10.1029/2010GL044696

Guan, B., & Waliser, D. (2019, 12). Tracking atmospheric rivers globally: Spatial distributions and temporal evolution of life cycle characteristics. *Journal of Geophysical Research: Atmospheres*, *124*. doi: 10.1029/2019JD031205

Guan, B., & Waliser, D. E. (2015). Detection of atmospheric rivers: Evaluation and application of an algorithm for global studies. *Journal of Geophysical Research: Atmospheres*, *120*(24), 12514-12535. Retrieved from https://agupubs.onlinelibrary.wiley.com/doi/abs/10.1002/2015JD024257 doi: https://doi.org/10.1002/2015JD024257

Harald, S., & Andreas, S. (2013). Moisture origin and meridional transport in atmospheric rivers and their association with multiple cyclones. *Monthly Weather Review*, *141*(8), 2850 - 2868. Retrieved from https://journals.ametsoc.org/view/journals/mwre/141/8/mwr-d-12-00256.1.xml doi: 10.1175/MWR-D-12-00256.1

Hegyi, B. M., & Taylor, P. C. (2018). The unprecedented 2016–2017 arctic sea ice growth season: The crucial role of atmospheric rivers and longwave fluxes. *Geophysical Research Letters*, *45*(10), 5204-5212. Retrieved from https://agupubs.onlinelibrary.wiley.com/doi/abs/10.1029/2017GL076717 doi: https://doi.org/10.1029/2017GL076717

Jasek, M. (1998, July 27–31). 1998 break-up and flood on the yukon river at dawson – did el niño and climate change play a role? In H. Shen (Ed.), *Ice in surface waters: Proceedings of the 14th international symposium on ice* (pp. 761–768). Rotterdam: A.A. Balkema.

Kalnay, E., Kanamitsu, M., Kistler, R., Collins, W., Deaven, D., Gandin, L., … Joseph, D. (1996). The ncep/ncar 40-year reanalysis project. *Bulletin of the American Meteorological Society*, *77*(3), 437 - 472. Retrieved from https://journals.ametsoc.org/view/journals/bams/77/3/1520-0477_1996_077_0437_tnyrp_2_0_co_2.xml doi: 10.1175/1520-0477(1996)077⟨0437:TNYRP⟩2.0.CO;2

Lashkari, H., & Esfandiari, N. (2020, 05). Identifying atmospheric river events and their paths into iran. *Theoretical and Applied Climatology*, *140*. doi: 10.1007/s00704-020-03148-w

Lavers, D. A., Allan, R. P., Villarini, G., Lloyd-Hughes, B., Brayshaw, D. J., & Wade, A. J. (2013). Future changes in atmospheric rivers and their implications for winter flooding in britain. *Environmental Research Letters*, *8*(3). Retrieved from https://doi.org/10.1088/1748-9326/8/3/034010 doi: 10.1088/1748-9326/8/3/034010

Lavers, D. A., Allan, R. P., Wood, E. F., Villarini, G., Brayshaw, D. J., & Wade, A. J. (2011). Winter floods in britain are connected to atmospheric rivers. *Geophysical Research Letters*, *38*(23). Retrieved from https://agupubs.onlinelibrary.wiley.com/doi/abs/10.1029/2011GL049783 doi:

https://doi.org/10.1029/2011GL049783
Li, L., Cannon, F., Mazloff, M. R., Subramanian, A. C., Wilson, A. M., & Ralph, F. M. (2022). Impact of atmospheric rivers on arctic sea ice variations. *EGUsphere*, *2022*, 1–21. Retrieved from https://egusphere.copernicus.org/preprints/2022/egusphere-2022-36/ doi: 10.5194/egusphere-2022-36
Little, K., Kingston, D. G., Cullen, N. J., & Gibson, P. B. (2019). The role of atmospheric rivers for extreme ablation and snowfall events in the southern alps of new zealand. *Geophysical Research Letters*, *46*(5), 2761-2771. Retrieved from https://agupubs.onlinelibrary.wiley.com/doi/abs/10.1029/2018GL081669 doi: https://doi.org/10.1029/2018GL081669
Ma, W., Wang, H., Chen, G., Qian, Y., Baxter, I., Huo, Y., & Seefeldt, M. W. (2023). Wintertime extreme warming events in the high arctic: Characteristics, drivers, trends, and the role of atmospheric rivers. *EGUsphere*. Retrieved from https://doi.org/10.5194/egusphere-2023-2018 (Preprint) doi: 10.5194/egusphere-2023-2018
Maclennan, M. L., Lenaerts, J. T. M., Shields, C., & Wille, J. D. (2022a). Contribution of atmospheric rivers to antarctic precipitation. *Geophysical Research Letters*, *49*(18), e2022GL100585. Retrieved from https://agupubs.onlinelibrary.wiley.com/doi/abs/10.1029/2022GL100585 (e2022GL100585 2022GL100585) doi: https://doi.org/10.1029/2022GL100585
Maclennan, M. L., Lenaerts, J. T. M., Shields, C., & Wille, J. D. (2022b). Contribution of atmospheric rivers to antarctic precipitation. *Geophysical Research Letters*, *49*(18). Retrieved 2024-04-16, from https://onlinelibrary.wiley.com/doi/abs/10.1029/2022GL100585 doi: 10.1029/2022GL100585
Massoud, E., Espinoza, V., Guan, B., & Waliser, D. (2019). Global climate model ensemble approaches for future projections of atmospheric rivers. *Earth's Future*, *7*(10), 1136-1151. Retrieved from https://agupubs.onlinelibrary.wiley.com/doi/abs/10.1029/2019EF001249 doi: https://doi.org/10.1029/2019EF001249
Massoud, E., Massoud, T., Guan, B., Sengupta, A., Espinoza, V., De Luna, M., … Waliser, D. (2020). Atmospheric rivers and precipitation in the middle east and north africa (mena). *Water*, *12*(10). Retrieved from https://www.mdpi.com/2073-4441/12/10/2863 doi: 10.3390/w12102863
Mattingly, K. S., Mote, T. L., & Fettweis, X. (2018). Atmospheric river impacts on greenland ice sheet surface mass balance. *Journal of Geophysical Research: Atmospheres*, *123*(16), 8538-8560. Retrieved from https://agupubs.onlinelibrary.wiley.com/doi/abs/10.1029/2018JD028714 doi: https://doi.org/10.1029/2018JD028714
Murphy, J. M., Garcia, S., Piston, A., Moss, J. H., Howard, K., Fergusson, E. A., … others (2022). Coastal surveys in alaska and their application to salmon run-size and harvest forecasts. *North Pacific Anadromous Fish Commission Technical Report*(18).
Nash, D., Rutz, J. J., & Jacobs, A. (2024). Atmospheric rivers in southeast alaska: Meteorological conditions associated with extreme precipitation. *Journal of Geophysical Research: Atmospheres*, *129*(4), e2023JD039294. Retrieved from https://agupubs.onlinelibrary.wiley.com/doi/abs/10.1029/2023JD039294 (e2023JD039294 2023JD039294) doi: https://doi.org/10.1029/2023JD039294
Neiman, P. J., Ralph, F. M., Wick, G. A., Kuo, Y.-H., Wee, T.-K., Ma, Z., … Dettinger, M. D. (2008). Diagnosis of an intense atmospheric river impacting the pacific northwest: Storm summary and offshore vertical structure observed with cosmic satellite retrievals. *Monthly Weather Review*, *136*(11), 4398 - 4420. Retrieved from https://journals.ametsoc.org/view/journals/mwre/136/11/2008mwr2550.1.xml doi: 10.1175/2008MWR2550.1
Paily, P., Macagno, E., & Kennedy, J. (1974, 3). Winter-regime surface heat loss

from heated streams. research report. *US Office of Scientific and Technical Information*. Retrieved from https://www.osti.gov/biblio/7179276

Paul J., N., Lawrence J., S., F. Martin, R., Mimi, H., & Gary A., W. (2011). Flooding in western washington: The connection to atmospheric rivers. *Journal of Hydrometeorology*, *12*(6), 1337 - 1358. Retrieved from https://journals.ametsoc.org/view/journals/hydr/12/6/2011jhm1358_1.xml doi: 10.1175/2011JHM1358.1

Prowse, T., Bonsal, B., Duguay, C., & Lacroix, M. (2007). River-ice break-up/freeze-up: a review of climatic drivers, historical trends and future predictions. *Annals of Glaciology*, *46*, 443–451. doi: 10.3189/172756407782871431

Prowse, T. D., & Beltaos, S. (2002). Climatic control of river-ice hydrology: a review. *Hydrological Processes*, *16*(4), 805-822. Retrieved from https://onlinelibrary.wiley.com/doi/abs/10.1002/hyp.369 doi: https://doi.org/10.1002/hyp.369

Ralph, F. M., Neiman, P. J., Wick, G. A., Gutman, S. I., Dettinger, M. D., Cayan, D. R., & White, A. B. (2006). Flooding on california's russian river: Role of atmospheric rivers. *Geophysical Research Letters*, *33*(13). Retrieved from https://agupubs.onlinelibrary.wiley.com/doi/abs/10.1029/2006GL026689 doi: https://doi.org/10.1029/2006GL026689

Rey, D., & Neuhauser, M. (2011). Wilcoxon-signed-rank test. In M. Lovric (Ed.), *International encyclopedia of statistical science* (pp. 1658–1659). Berlin, Heidelberg: Springer Berlin Heidelberg. Retrieved from https://doi.org/10.1007/978-3-642-04898-2_616 doi: 10.1007/978-3-642-04898-2_616

Saavedra, F., Cortés, G., Viale, M., Margulis, S., & McPhee, J. (2020). Atmospheric rivers contribution to the snow accumulation over the southern andes (26.5° s–37.5° s). *Frontiers in Earth Science*, *8*. Retrieved from https://www.frontiersin.org/articles/10.3389/feart.2020.00261 doi: 10.3389/feart.2020.00261

Saha, S., Moorthi, S., Pan, H.-L., Wu, X., Wang, J., Nadiga, S., … Goldberg, M. (2010). The ncep climate forecast system reanalysis. *Bulletin of the American Meteorological Society*, *91*(8), 1015 - 1058. Retrieved from https://journals.ametsoc.org/view/journals/bams/91/8/2010bams3001_1.xml doi: 10.1175/2010BAMS3001.1

Shapiro, S. S., & Wilk, M. B. (1965). An analysis of variance test for normality (complete samples). *Biometrika*, *52*(3-4), 591–611.

Shen, H. T. (2010). Mathematical modeling of river ice processes. *Cold Regions Science and Technology*, *62*(1), 3-13. Retrieved from https://www.sciencedirect.com/science/article/pii/S0165232X10000339 doi: https://doi.org/10.1016/j.coldregions.2010.02.007

Thornton, M., Shrestha, R., Wei, Y., Thornton, P., Kao, S.-C., & Wilson, B. (2022). *Daymet: Annual climate summaries on a 1-km grid for north america, version 4 r1.* ORNL Distributed Active Archive Center. Retrieved from https://daac.ornl.gov/cgi-bin/dsviewer.pl?ds_id=2130 doi: 10.3334/ORNLDAAC/2130

Thornton, P. E., Shrestha, R., Thornton, M., Kao, S.-C., Wei, Y., & Wilson, B. E. (2021, 7 23). Gridded daily weather data for north america with comprehensive uncertainty quantification. *Scientific Data*, *8*(1), 190. Retrieved from https://doi.org/10.1038/s41597-021-00973-0 doi: 10.1038/s41597-021-00973-0

Viale, M., Valenzuela, R., Garreaud, R. D., & Ralph, F. M. (2018). Impacts of atmospheric rivers on precipitation in southern south america. *Journal of Hydrometeorology*, *19*(10), 1671 - 1687. Retrieved from https://journals.ametsoc.org/view/journals/hydr/19/10/jhm-d-18-0006_1.xml doi: 10.1175/JHM-D-18-0006.1

Wang, Z., Ding, Q., Wu, R., Ballinger, T. J., Guan, B., Bozkurt, D., … Chen,

Z. (2024, June 29). Role of atmospheric rivers in shaping long term arctic moisture variability. *Nature Communications*, *15*(1), 5505. Retrieved from https://doi.org/10.1038/s41467-024-49857-y doi: 10.1038/s41467-024-49857-y

Wille, J. D., Favier, V., Gorodetskaya, I. V., Agosta, C., Kittel, C., Beeman, J. C., … Codron, F. (2021). Antarctic atmospheric river climatology and precipitation impacts. *Journal of Geophysical Research: Atmospheres*, *126*(8), e2020JD033788. Retrieved from https://agupubs.onlinelibrary.wiley.com/doi/abs/10.1029/2020JD033788 (e2020JD033788 2020JD033788) doi: https://doi.org/10.1029/2020JD033788

Zhang, P., Chen, G., Ting, M., Ruby Leung, L., Guan, B., & Li, L. (2023, March). More frequent atmospheric rivers slow the seasonal recovery of arctic sea ice. *Nature Climate Change*, *13*(3), 266–273. Retrieved from https://doi.org/10.1038/s41558-023-01599-3 doi: 10.1038/s41558-023-01599-3

Zhu, Y., & Newell, R. E. (1998). A proposed algorithm for moisture fluxes from atmospheric rivers. *Monthly Weather Review*, *126*(3), 725 - 735. Retrieved from https://journals.ametsoc.org/view/journals/mwre/126/3/1520-0493_1998_126_0725_apafmf_2.0.co_2.xml doi: 10.1175/1520-0493(1998)126⟨0725:APAFMF⟩2.0.CO;2

Appendix A.

Table 1. Table showing the Pearson correlation coefficients between the total thermal energy exchange (Q) as derived by Equation 3, assuming an exponential temporal bias (Equation 2), and the day of the year the breakup occured (DOY), by location. The optimal center placement of the temporal bias (month-day) is also provided [r_p|center date of bias]

Location	**Total Precipitation**	**Precipitation from ARs**	**Precipitation not from ARs**
Akiak Kuskokwim River	−0.78|11-12	−0.78|2-5	−0.80|1-15
Allakaket Koyukuk River	−0.81|12-10	−0.69|10-23	−0.80|12-3
Ambler Kobuk River	−0.84|2-5	−0.67|2-5	−0.83|2-12
Aniak Kuskokwim River	−0.80|11-19	−0.81|1-29	−0.77|11-12
Bethel Kuskokwim River	−0.72|12-3	−0.75|2-5	−0.73|12-10
Bettles Koyukuk River	−0.79|2-19	−0.70|10-23	−0.81|2-12
Circle Yukon River	−0.75|2-5	−0.76|1-22	−0.74|2-12
Crooked Creek Kuskokwim River	−0.84|11-26	−0.76|2-5	−0.80|11-26
Dawson Yukon River	−0.77|10-23	−0.67|1-22	−0.75|10-23
Eagle Yukon River	−0.77|10-23	−0.79|1-22	−0.76|1-29
Emmonak Yukon River	−0.76|2-5	−0.76|1-29	−0.71|4-16
Fort Yukon Yukon River	−0.72|10-23	−0.59|2-5	−0.72|10-23
Galena Yukon River	−0.79|11-19	−0.75|1-15	−0.80|4-16
Holy Cross Yukon River	−0.75|1-8	−0.77|1-8	−0.72|1-8
Hughes Koyukuk River	−0.81|1-1	−0.78|1-15	−0.78|4-2
Kaltag Yukon River	−0.84|12-3	−0.77|12-3	−0.86|1-15
Kobuk Kobuk River	−0.81|1-8	−0.62|4-16	−0.81|1-8
McGrath Kuskokwim River	−0.81|3-26	−0.81|2-5	−0.82|4-9
Mountain Village Yukon River	−0.72|1-29	−0.76|2-5	−0.69|2-19
Nenana Tanana River	−0.71|1-1	−0.73|2-5	−0.72|1-1
Nikolai Kuskokwim River	−0.75|2-12	−0.70|2-5	−0.74|1-15
Red Devil Kuskokwim River	−0.79|12-3	−0.80|2-5	−0.78|12-3
Ruby Yukon River	−0.83|4-9	−0.78|1-15	−0.86|4-16
Russian Mission Yukon River	−0.71|11-26	−0.72|12-10	−0.68|12-3
Tanana Yukon River	−0.76|1-22	−0.70|2-5	−0.77|11-26